

Charged line segments and ellipsoidal equipotentials

T L Curtright[§], N M Aden, X Chen, M J Haddad, S Karayev, D B Khadka, and J Li
Department of Physics, University of Miami
Coral Gables, FL 33124-8046, USA

[§]curtright@miami.edu

January 18, 2016

Abstract

This is a survey of the electrostatic potentials produced by charged straight-line segments, in various numbers of spatial dimensions, with comparisons between uniformly charged segments and those having non-uniform linear charge distributions that give rise to ellipsoidal equipotentials surrounding the segments. A uniform linear distribution of charge is compatible with ellipsoidal equipotentials only for three dimensions. In higher dimensions, the linear charge density giving rise to ellipsoidal equipotentials is counter-intuitive — the charge distribution has a maximum at the center of the segment and vanishes at the ends of the segment. Only in two dimensions is the continuous charge distribution intuitive — for that one case of ellipsoidal equipotentials, the charge is peaked at the ends of the segment and minimized at the center.

Contents

1	Introduction	1
2	Electrostatics in two dimensions	2
3	Point charge in D dimensions	13
4	Uniformly charged line segments for all dimensions $D > 2$	14
5	Ellipsoidal equipotentials for all dimensions $D > 2$	19
6	Generalizations	25
7	Summary	26

1 Introduction

It has become a widespread practice to study the physics of systems in various numbers of spatial dimensions, not necessarily $D = 3$. For instance, graphene with $D = 2$, and string or membrane theory with D as high as 25, are two examples that immediately come to mind for both their experimental and theoretical interest. Moreover, geometric ideas provide a common framework used to pursue such studies. A pedagogical goal of this paper is to encourage students to think along these lines in the context of a familiar subject — electrostatics.

For example, in three spatial dimensions a uniformly charged straight-line segment gives rise to an electric potential Φ whose equipotential surfaces are prolate ellipsoids of revolution about the segment, with the ends of the segment providing the foci of the ellipsoid. As an immediate consequence of the geometry for these prolate ellipsoidal equipotentials, the associated electric field $\vec{E} = -\vec{\nabla}\Phi$ — always normal to surfaces of constant Φ — has at any observation point a direction that bisects the angle formed by the pair of lines from the observation point to each of the two foci of the ellipsoid. This beautiful electrostatic example was presented by George Green in 1828 [1], and it has been discussed in many books since then [2]-[10] including at least two texts from this century [11]. While the straight-line segment is an idealization, nevertheless it provides insight into the behavior of real thin-wire conductors, especially upon approximating those real wires as very narrow, “needle-like” ellipsoids.

But as it turns out, the line segment problem in three dimensions is a very special case, in some sense the most ideal of all possible electrostatic worlds. In any *other* dimension of space, uniformly charged segments do **not** produce ellipsoidal equipotentials. Conversely, in any other dimension, if the equipotentials are ellipsoidal about a linearly distributed straight-line segment of charge, then that charge distribution can **not** be uniform.

One need look no farther than two dimensional systems to see clearly that there are differences between uniformly charged segments and those with charge distributed so as to produce ellipsoidal equipotentials. Indeed, $D = 2$ is the only ellipsoidal equipotential case which is intuitive in the sense that the associated linear charge distribution has maxima at the ends of the segment, as one might naively expect from the repulsive force between like charges placed on a segment of a real, thin conductor at a finite potential. In contrast, the distribution of charge needed to produce ellipsoidal equipotentials is counter-intuitive in higher dimensions. To produce such equipotentials for $D > 3$ the charge distribution must have a maximum at the center and vanish at the ends of the segment.

We begin our discussion in Section 2 in two dimensions, where the two types of charged segments are readily analyzed. Then we compare and contrast uniformly charged line segments with those admitting ellipsoidal equipotentials for any number of spatial dimensions. As a preliminary, we first discuss briefly in Section 3 the potential of a point charge in D dimensions. We then use this information in Section 4 to compute the potentials and electric fields for uniformly charged line segments. We continue in Section 5 by considering systems with ellipsoidal equipotentials in D dimensions. We then determine the linear charge distributions that produce such potential configurations, and we find the remarkable result that the linear charge density giving rise to ellipsoidal equipotentials is peaked at the center of the segment, for $D > 3$.

The discussion of general D affords the opportunity to illustrate how continuous D can be used as a mathematical device to regulate singular behavior. This too is a widespread practice in theoretical physics. We use D in this way in Section 5 of the paper to interpolate continuously between intuitive and counter-intuitive charge distributions for segments with ellipsoidal equipotentials.

Finally, in Section 6, we invoke well-known methods to indicate how the various line segment results also give solutions to a class of electrostatic boundary value problems where the charge is moved outward and distributed on one of the equipotential surfaces that surrounds the original segment.

2 Electrostatics in two dimensions

The point-particle electric potential in 2D is well-known to be logarithmic. For a point charge Q located at the origin, up to a constant R that sets the distance scale,

$$\Phi_{\text{point}}(\vec{r}) = kQ \ln(R/r) , \quad \nabla^2 \Phi_{\text{point}}(\vec{r}) = -2\pi kQ \delta^2(\vec{r}) , \quad (1)$$

where k is the two dimensional analogue of Coulomb’s constant.

By linear superposition, a finite length, uniformly charged line segment, with constant charge/length λ distributed on the x axis for $-L/2 \leq x \leq L/2$, produces a potential

$$\Phi_{\text{line}}(x, y) = -k\lambda \left(u \ln \sqrt{u^2 + y^2} - u + y \arctan \frac{u}{y} \right) \Big|_{u=-x-L/2}^{u=-x+L/2} + k\lambda L \ln(R) . \quad (2)$$

This result may be established by integrating the contributions of infinitesimal point-like bits of charge that make up the segment, using (1) and the indefinite integral

$$\int \ln(\sqrt{u^2 + y^2}) du = u \ln(\sqrt{u^2 + y^2}) - u + y \arctan \frac{u}{y} . \quad (3)$$

Written out in full,

$$\begin{aligned} \Phi_{\text{line}}(x, y) = & k\lambda \left(L + y \arctan\left(\frac{x - \frac{1}{2}L}{y}\right) - y \arctan\left(\frac{x + \frac{1}{2}L}{y}\right) \right) \\ & + \left(x - \frac{1}{2}L\right) k\lambda \ln\left(\frac{1}{R} \sqrt{\left(x - \frac{1}{2}L\right)^2 + y^2}\right) - \left(x + \frac{1}{2}L\right) k\lambda \ln\left(\frac{1}{R} \sqrt{\left(x + \frac{1}{2}L\right)^2 + y^2}\right) . \end{aligned} \quad (4)$$

A plot of the potential surface shows the essential features.

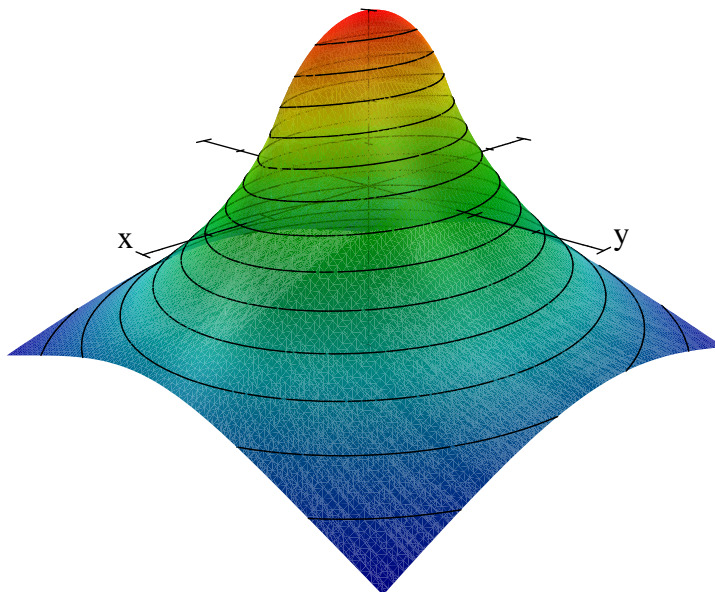


Figure 1: Potential surface for a uniformly charged line segment in 2D.

The top of the potential surface is curved and not a straight line, indicating that the charged segment itself is *not* an equipotential. This follows analytically from (4). Although points on the segment are not at the *same* potential, they are all at *finite* values of the potential, for $D = 2$. Explicitly, for $y = 0$ and all x ,

$$\Phi_{\text{line}}(x, 0) = k\lambda L - k\lambda \left(\frac{1}{2}L + x\right) \ln\left(\left|\frac{1}{2}L + x\right|/R\right) - k\lambda \left(\frac{1}{2}L - x\right) \ln\left(\left|\frac{1}{2}L - x\right|/R\right) . \quad (5)$$

We plot $f(x) = \Phi_{\text{line}}(x, 0)/k\lambda$ versus x to show the shape of the potential along the x -axis, for $L = 2$ and $R = 1$.

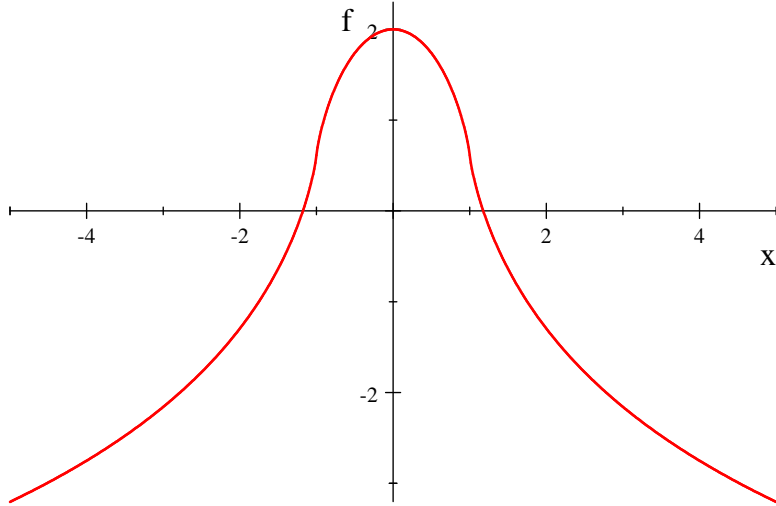


Figure 2: Uniformly charged line segment potential for $D = 2$, along the x -axis.

On the other hand, transverse to the x -axis the potential has a discontinuous slope across the line segment. That is to say, the electric field normal to the line segment, E_y , is discontinuous due to the presence of the charge density on the segment. For example, for $x = 0$ this transverse profile is given by

$$\Phi(0, y) = k\lambda \left[L - L \ln \left(\sqrt{\frac{1}{4}L^2 + y^2/R} \right) - 2y \arctan \left(\frac{1}{2}L/y \right) \right]. \quad (6)$$

We also plot $g(y) = \Phi_{\text{line}}(0, y) / k\lambda$ versus y to show the shape of the potential along the y -axis, for $L = 2$ and $R = 1$.

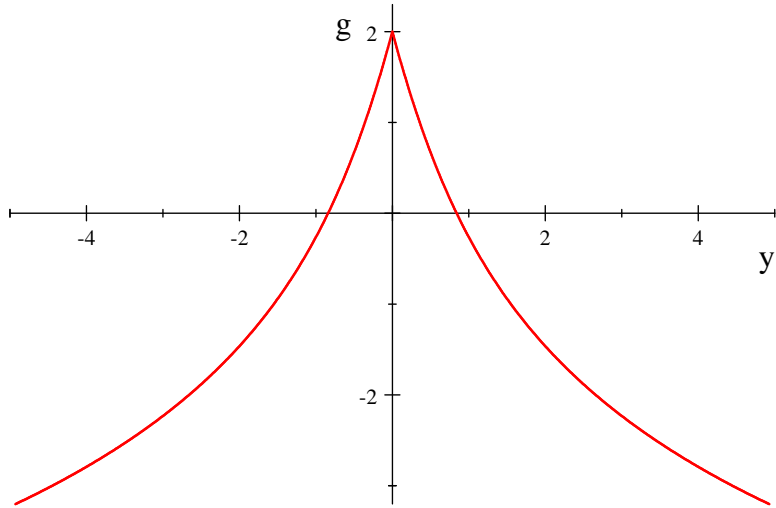


Figure 3: Uniformly charged line segment potential for $D = 2$, along the y -axis.

Moreover, the equipotentials are *not* ellipses surrounding the segment on the xy -plane, as is especially clear for points close to the segment. The potential contours actually *intersect* the segment. A view of the potential contours from *below* the potential surface shows these features graphically. (See the plot to follow. But note the view in that plot is actually an orthogonal projection of the contours onto the xy -plane, and not the true perspective of an observer on the potential axis a finite distance below that plane.)

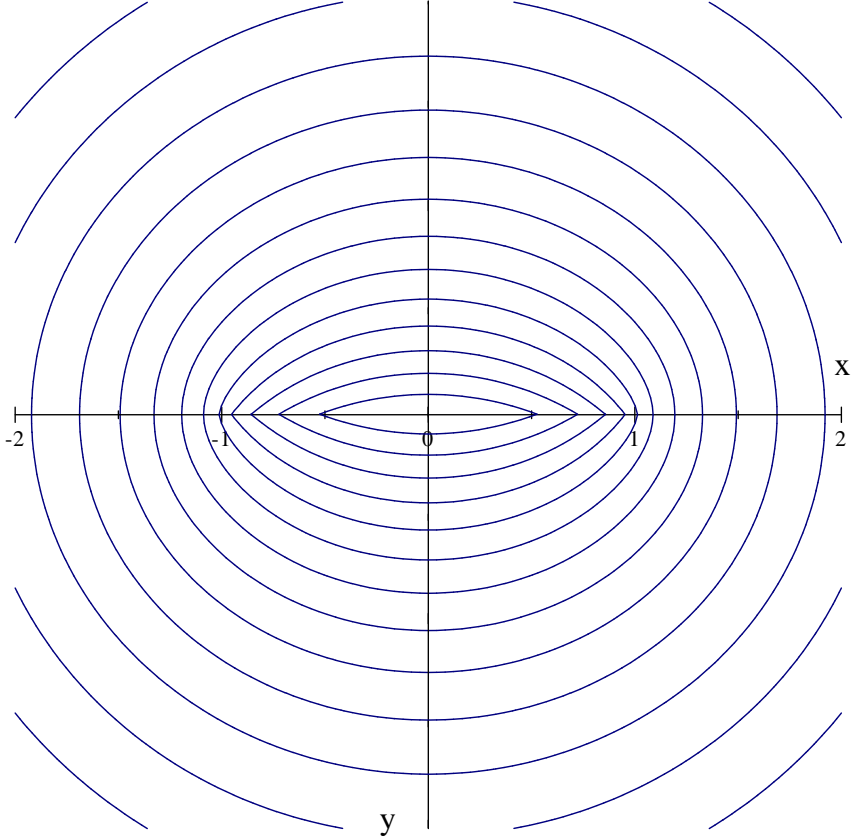


Figure 4: Potential contours for a uniformly charged line segment in 2D.

The components of the electric field produced by the segment are given by

$$E_x(x, y) = -\frac{\partial}{\partial x} \Phi_{\text{line}}(x, y) = k\lambda \ln \left(\sqrt{\frac{(x + \frac{1}{2}L)^2 + y^2}{(x - \frac{1}{2}L)^2 + y^2}} \right), \quad (7)$$

$$E_y(x, y) = -\frac{\partial}{\partial y} \Phi_{\text{line}}(x, y) = k\lambda \arctan \left(\frac{L + 2x}{2y} \right) + k\lambda \arctan \left(\frac{L - 2x}{2y} \right), \quad (8)$$

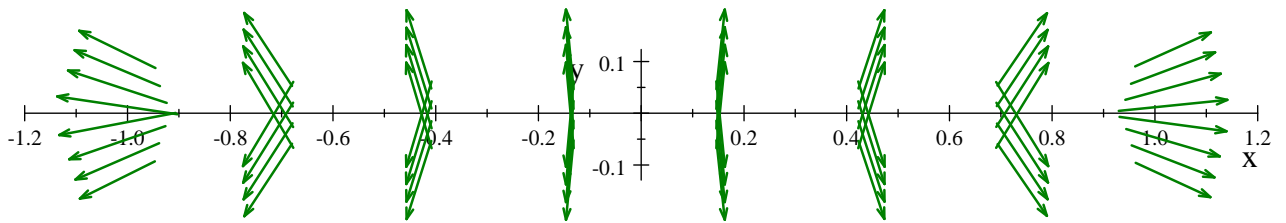
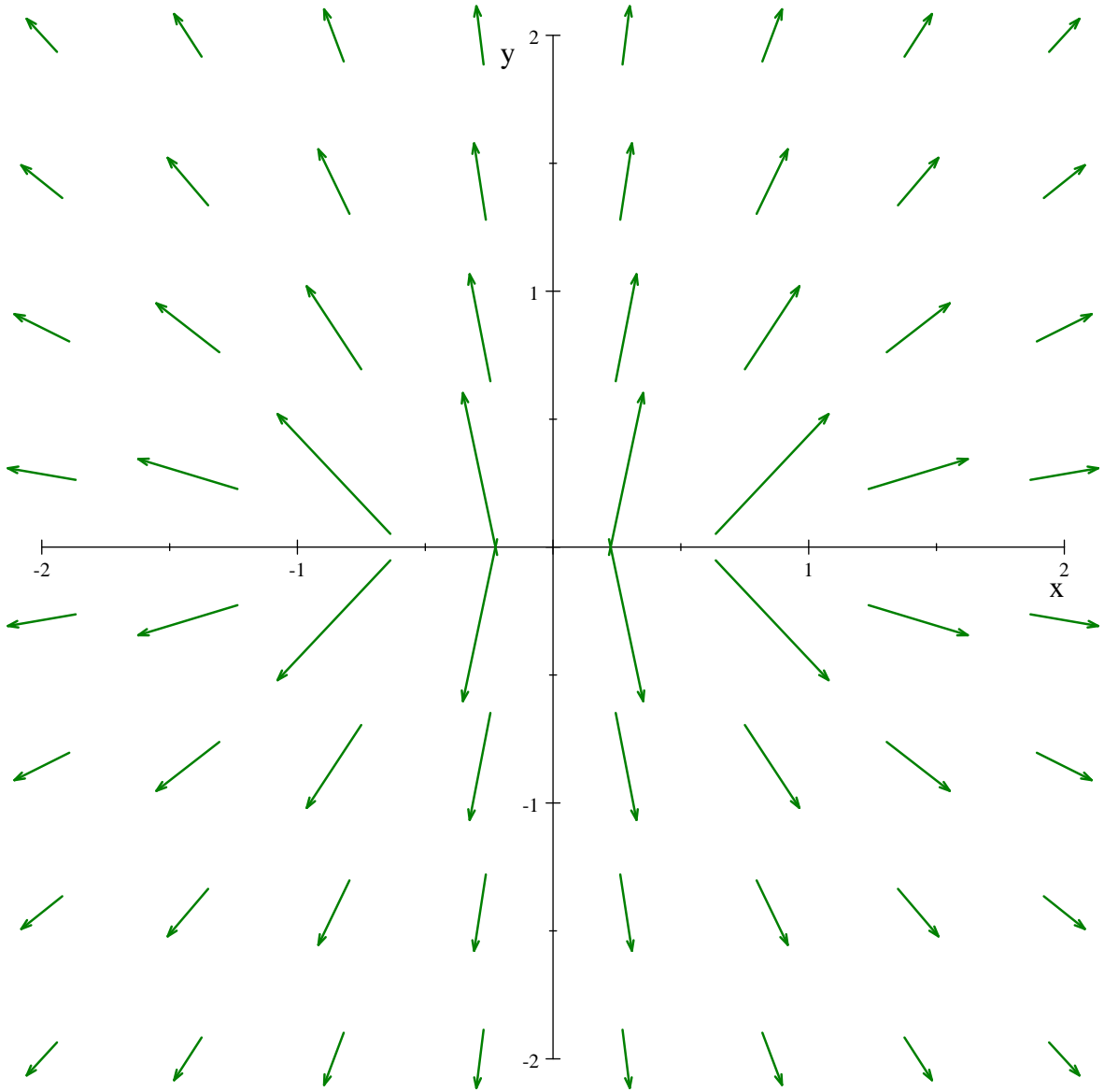
where we have used $\frac{d}{du} \arctan u = \frac{1}{u^2+1}$. Note that $\vec{E}(x, y)$ is independent of the scale R , since changing R just amounts to adding a constant to the potential. But of course $\vec{E}(x, y)$ does depend on L as this sets the physical length scale for the system.

As a check, in the units we have chosen the charge density along the line follows from $\int \vec{\nabla} \cdot \vec{E} \, dx dy = 2\pi k \int \rho \, dx dy$, integrated over a horizontal rectangle containing an infinitesimal portion of the x -axis, as the height of the rectangle is taken to zero. Thus, using $\lim_{z \rightarrow \pm\infty} \arctan z = \pm\pi/2$,

$$2\pi k \lambda(x) = 2 \lim_{y \rightarrow 0} E_y(x, y) = 2k\lambda \times \begin{cases} 0 & \text{if } x > L/2 \\ \pi & \text{if } -L/2 < x < L/2 \\ 0 & \text{if } x < -L/2 \end{cases}. \quad (9)$$

That is to say, the charge/length between $-L/2$ and $L/2$ is the constant λ , as expected. Elsewhere, the charge density vanishes, as follows from $\nabla^2 \Phi_{\text{line}}(\vec{r}) = 0$ for all points not coincident with the segment.

It is instructive to make a vector field plot of $(E_x(x, y), E_y(x, y))$, especially near the charged segment. Again it is evident graphically that the segment itself is not an equipotential, since the electric field lines are not perpendicular to the segment as the x -axis is approached for $-L/2 < x < L/2$, except at the single point $x = 0$. Here are vector field plots for $L = 2$.



Figures 5 & 6: Vector field plots of \vec{E} for a uniformly charged line segment situated between $x = -1$ and $x = +1$. The field is evaluated at the center of each arrow.

In contrast to the uniformly charged segment in 2D, consider a distribution of charge along the segment such that equipotentials *are* ellipsoidal. The relevant charge distribution turns out to be

$$\lambda(x) = \frac{2\lambda L}{\pi} \frac{1}{\sqrt{L^2 - 4x^2}} \begin{cases} 0 & \text{if } x > L/2 \\ 1 & \text{if } -L/2 < x < L/2 \\ 0 & \text{if } x < -L/2 \end{cases}, \quad (10)$$

as we shall confirm in the following. Since $\int_{-1}^1 \frac{1}{\sqrt{1-s^2}} ds = \pi$, the total charge on the segment is still $Q = \int_{-L/2}^{L/2} \lambda(x) dx = \lambda L$, the same as for the uniformly charged case.

The corresponding potential is now

$$\Phi_{\text{line}}(x, y) = k\lambda L \ln \left(\frac{4R}{s + \sqrt{s^2 - L^2}} \right), \quad (11)$$

where s is a sum of two distances, from the observation point (x, y) to each of the two ends of the segment. That is,

$$s = r_- + r_+, \quad r_{\pm} = \sqrt{\left(x \pm \frac{1}{2}L\right)^2 + y^2}. \quad (12)$$

Because the positional dependence of the potential is given entirely by s , the equipotentials are ellipses in the xy -plane, with the ends of the segment serving as the foci of each equipotential ellipse. Again, we plot the potential surface.

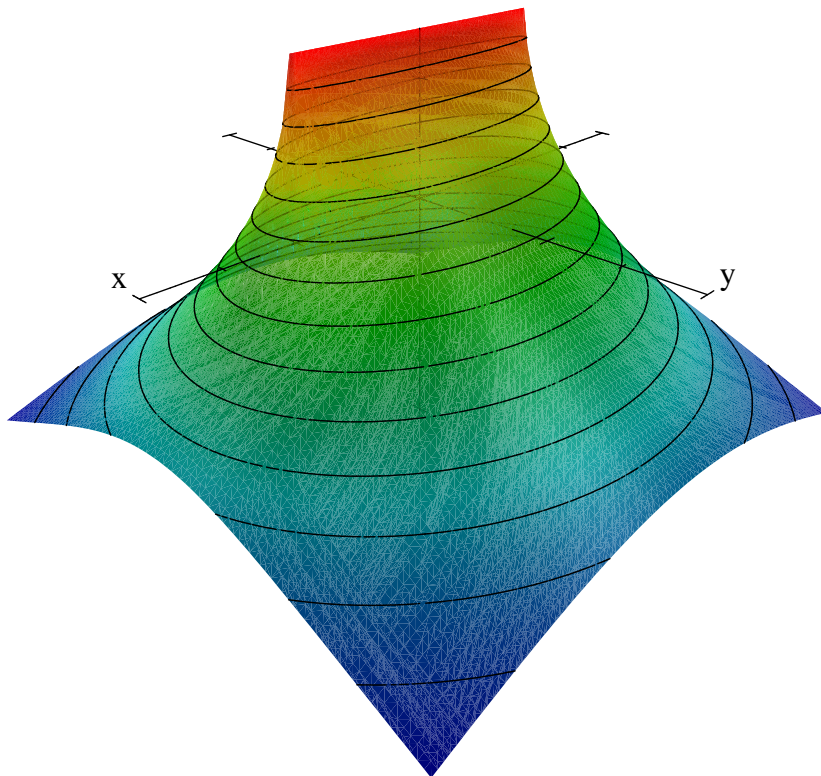


Figure 7: Potential surface for a non-uniformly charged line segment in 2D, with $\lambda(x) = \frac{2\lambda L/\pi}{\sqrt{L^2 - 4x^2}}$.

The top of the potential surface is now a straight line, indicating that the charged segment itself *is* an equipotential, and the points on the segment are at a *finite* potential for $D = 2$, namely, $\Phi = k\lambda L \ln(4R/L)$.

This follows analytically from (11). Explicitly, for $y = 0$ and all x ,

$$\Phi_{\text{line}}(x, 0) = k\lambda L \ln \left(\frac{4R}{|x - \frac{1}{2}L| + |x + \frac{1}{2}L| + \sqrt{2(x^2 - \frac{1}{4}L^2 + |x^2 - \frac{1}{4}L^2|)}} \right). \quad (13)$$

We plot $f(x) = \frac{1}{k\lambda} \Phi_{\text{line}}(x, 0)$ versus x to show the shape of the potential along the x -axis, for $L = 2$ and $R = 1$.

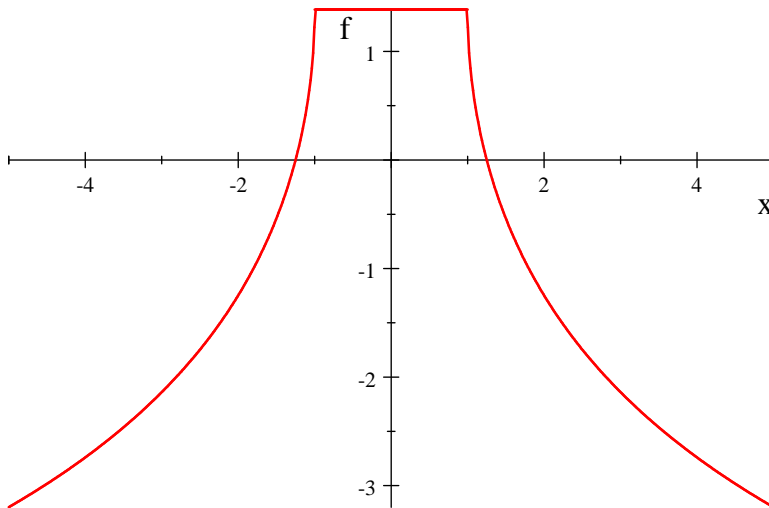


Figure 8: Non-uniformly charged line segment potential for $D = 2$, along the x -axis.

Transverse to the x -axis, the potential again has a discontinuous slope across the line segment due to the presence of the charge density on the segment. For example, for $x = 0$ this transverse profile is given by

$$\Phi_{\text{line}}(0, y) = Lk\lambda \ln \left(\frac{4R}{\sqrt{L^2 + 4y^2} + 2|y|} \right). \quad (14)$$

We plot $g(y) = \frac{1}{k\lambda} \Phi_{\text{line}}(0, y)$ versus y to show the shape of the potential along the y -axis, for $L = 2$ and $R = 1$.

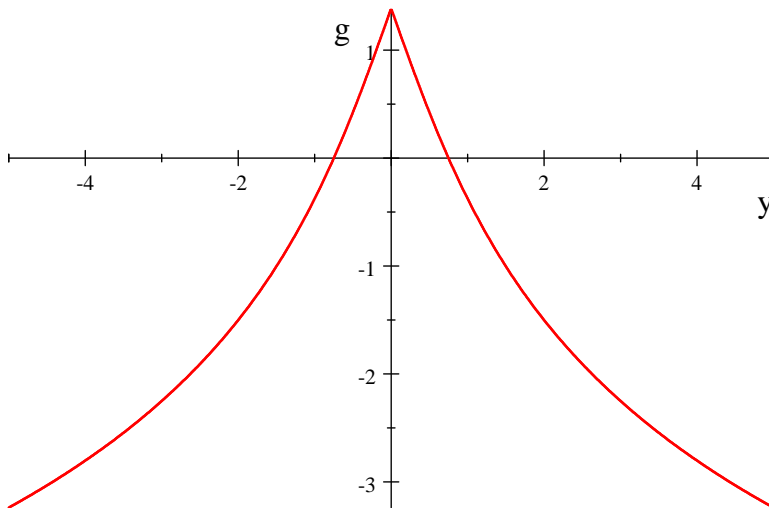


Figure 9: Non-uniformly charged line segment potential for $D = 2$, along the y -axis.

A view of the potential contours from below the potential surface shows the equipotential ellipses. (But again note the view in that plot is actually an orthogonal projection of the contours onto the xy -plane, and not the true perspective of an observer on the potential axis a finite distance below that plane.)

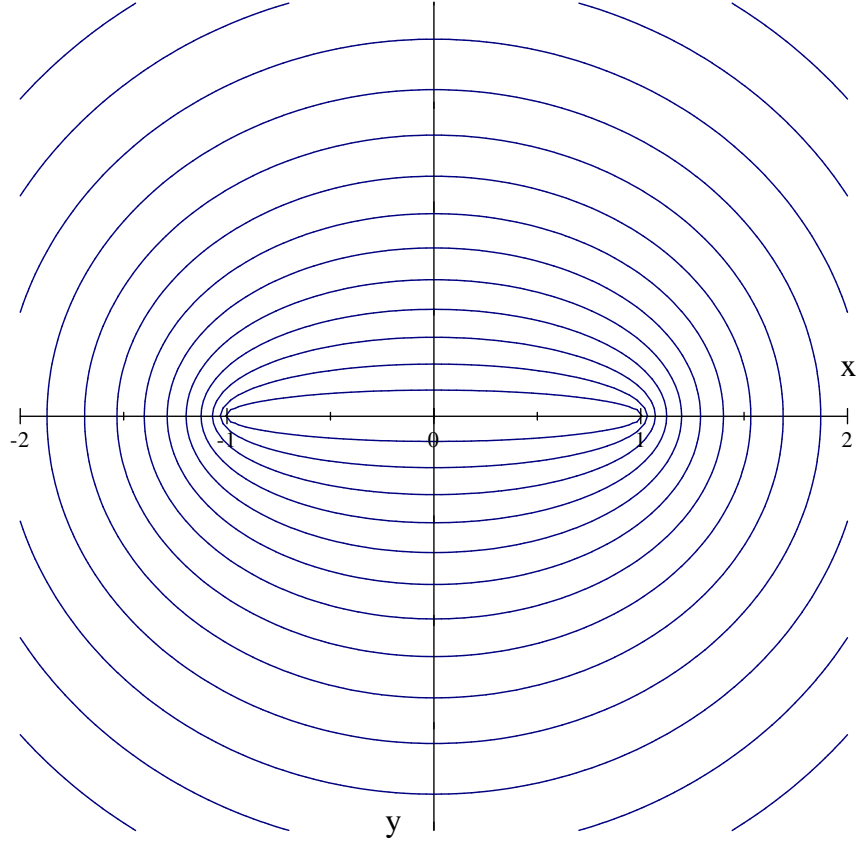


Figure 10: Ellipsoidal potential contours for a non-uniformly charged line segment in 2D.

The components of the electric field are now

$$E_x(x, y) = -\frac{\partial}{\partial x} \Phi_{\text{line}}(x, y) = \frac{k\lambda L}{\sqrt{s^2 - L^2}} \frac{\partial s}{\partial x}, \quad (15)$$

$$E_y(x, y) = -\frac{\partial}{\partial y} \Phi_{\text{line}}(x, y) = \frac{k\lambda L}{\sqrt{s^2 - L^2}} \frac{\partial s}{\partial y}, \quad (16)$$

whose final form in rectangular coordinates follows from

$$\frac{\partial s}{\partial x} = \frac{x - \frac{1}{2}L}{r_-} + \frac{x + \frac{1}{2}L}{r_+} = \frac{1}{r_+ r_-} \left(s x - \frac{1}{2}(r_+ - r_-)L \right), \quad \frac{\partial s}{\partial y} = \frac{y}{r_-} + \frac{y}{r_+} = \frac{1}{r_+ r_-} s y. \quad (17)$$

In terms of x , y , r_+ , and r_- ,

$$E_x(x, y) = \frac{k\lambda L}{r_+ r_- \sqrt{(r_- + r_+)^2 - L^2}} \left(\left(x - \frac{1}{2}L \right) r_+ + \left(x + \frac{1}{2}L \right) r_- \right), \quad (18)$$

$$E_y(x, y) = \frac{k\lambda L}{r_+ r_- \sqrt{(r_- + r_+)^2 - L^2}} (r_- + r_+) y. \quad (19)$$

Writing everything out in terms of x and y gives

$$r_+ r_- = \sqrt{\left(\frac{1}{4} L^2 + x^2 + y^2\right)^2 - L^2 x^2}, \quad (r_- + r_+)^2 - L^2 = 2 \left(x^2 + y^2 - \frac{1}{4} L^2 + \sqrt{\left(\frac{1}{4} L^2 + x^2 + y^2\right)^2 - L^2 x^2} \right). \quad (20)$$

The components of \vec{E} are not elegant in these coordinates [13] but their properties are fully encoded and amenable to machine computation.

$$E_x(x, y) = \frac{k\lambda L}{\sqrt{2}} \frac{(x + \frac{1}{2} L) \sqrt{(x - \frac{1}{2} L)^2 + y^2} + (x - \frac{1}{2} L) \sqrt{(x + \frac{1}{2} L)^2 + y^2}}{\sqrt{\left(\frac{1}{4} L^2 + x^2 + y^2\right)^2 - L^2 x^2} \sqrt{x^2 + y^2 - \frac{1}{4} L^2 + \sqrt{\left(\frac{1}{4} L^2 + x^2 + y^2\right)^2 - L^2 x^2}}}, \quad (21)$$

$$E_y(x, y) = \frac{k\lambda L}{\sqrt{2}} \frac{\left(\sqrt{(x - \frac{1}{2} L)^2 + y^2} + \sqrt{(x + \frac{1}{2} L)^2 + y^2}\right) y}{\sqrt{\left(\frac{1}{4} L^2 + x^2 + y^2\right)^2 - L^2 x^2} \sqrt{x^2 + y^2 - \frac{1}{4} L^2 + \sqrt{\left(\frac{1}{4} L^2 + x^2 + y^2\right)^2 - L^2 x^2}}}. \quad (22)$$

Although the geometric features of the electric field may not be transparent from these expressions, nevertheless the fact that the equipotentials are ellipsoidal allows one to immediately visualize the direction of \vec{E} as normal to those surfaces of constant Φ .

To confirm the charge density along the line, we again use $\int \vec{\nabla} \cdot \vec{E} \, dx dy = 2\pi k \int \rho \, dx dy$, and integrate over a horizontal rectangle containing an infinitesimal portion of the x -axis, as the height of the rectangle is taken to zero. The crucial features here are $s - L \rightarrow |2x - L| > 0$ as $y \rightarrow 0$ for $|x| > L/2$ (away from the segment), but $s - L \rightarrow 0$ as $y \rightarrow 0$ for $-L/2 < x < L/2$ (on the segment). More precisely, as points on the segment are approached transversely,

$$s = \left(\frac{1}{2} L - x\right) \sqrt{1 + \frac{y^2}{\left(\frac{1}{2} L - x\right)^2}} + \left(\frac{1}{2} L + x\right) \sqrt{1 + \frac{y^2}{\left(\frac{1}{2} L + x\right)^2}} \\ \underset{y \rightarrow 0}{\sim} L + \frac{1}{2} \left(\frac{1}{\frac{1}{2} L - x} + \frac{1}{\frac{1}{2} L + x}\right) y^2 + O(y^4) = L + \frac{1}{2} L \left(\frac{1}{\frac{1}{4} L^2 - x^2}\right) y^2 + O(y^4). \quad (23)$$

Thus for $-L/2 < x < L/2$,

$$\lim_{y \rightarrow 0} \left(\frac{y}{\sqrt{s^2 - L^2}}\right) = \frac{1}{\sqrt{2L}} \lim_{y \rightarrow 0} \frac{y}{\sqrt{s - L}} = \frac{1}{\sqrt{2L}} \lim_{y \rightarrow 0} \frac{y}{\sqrt{\frac{1}{2} L \left(\frac{1}{\frac{1}{4} L^2 - x^2}\right) y^2}} = \frac{1}{L} \sqrt{\frac{1}{4} L^2 - x^2}. \quad (24)$$

Combining this with the more obvious $\lim_{y \rightarrow 0} (r_+ r_-) = \frac{1}{4} L^2 - x^2$ for $-L/2 < x < L/2$ gives

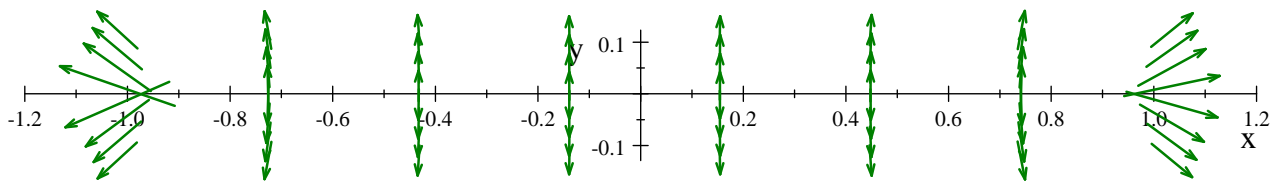
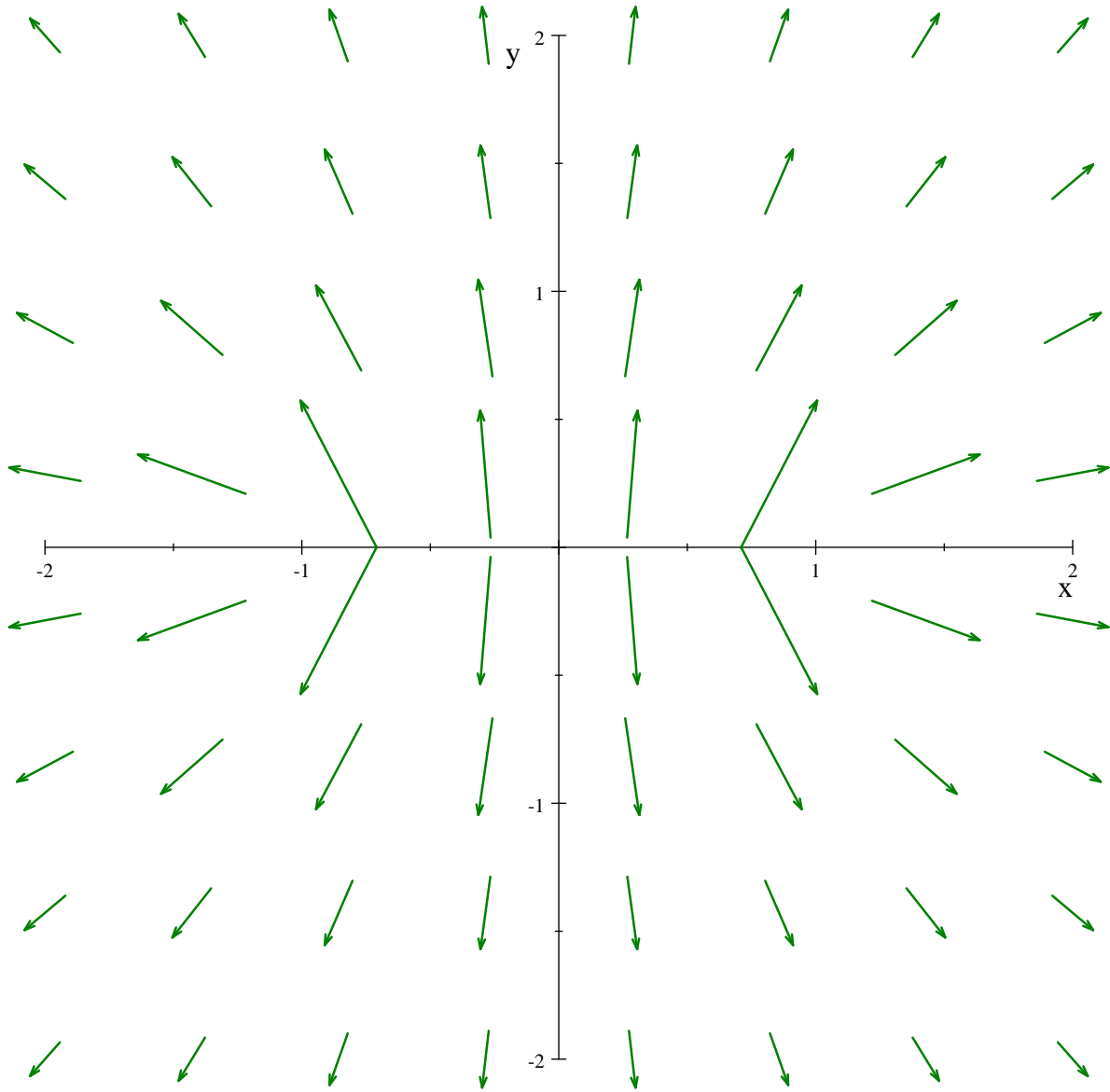
$$2\pi k \lambda(x) = 2 \lim_{y \rightarrow 0} E_y(x, y) = \lim_{y \rightarrow 0} \left(\frac{2k\lambda L s}{r_+ r_-} \frac{y}{\sqrt{s^2 - L^2}}\right) = \frac{2k\lambda L}{\sqrt{\frac{1}{4} L^2 - x^2}} \times \begin{cases} 0 & \text{if } x > L/2 \\ 1 & \text{if } -L/2 < x < L/2 \\ 0 & \text{if } x < -L/2 \end{cases}. \quad (25)$$

That is to say, the charge/length between $-L/2$ and $L/2$ is

$$\lambda(x) = \frac{2\lambda L}{\pi \sqrt{L^2 - 4x^2}}, \quad (26)$$

as anticipated above in (10). Elsewhere, the charge density vanishes, again as follows from $\nabla^2 \Phi_{\text{line}}(\vec{r}) = 0$ for all points not coincident with the segment.

Once more it is instructive to make a vector field plot of $(E_x(x, y), E_y(x, y))$, especially near the charged segment. The fact that the segment itself is an equipotential is evident graphically since the electric field lines are perpendicular to the segment as the x -axis is approached for $-L/2 < x < L/2$. Here are vector field plots for $L = 2$.



Figures 11 & 12: Vector field plots of \vec{E} for a non-uniformly charged line segment situated between $x = -1$ and $x = +1$. The field is evaluated at the center of each arrow.

As previously stressed, the geometry of the ellipsoidal equipotentials ensures that the electric field at any observation point always has a direction that bisects the angle formed by the two lines from the end points of the segment to the observation point [14]. This result is also manifest in an integral expression for \vec{E} that follows from linear superposition of the field contributions from infinitesimal $\lambda(x) dx$ charges along the segment, upon choosing an appropriate integration variable. That is,

$$\vec{E}(x, y) = \frac{k\lambda L \sqrt{\sin \theta_+ \sin \theta_-}}{\pi y} \int_{\frac{1}{2}(\theta_+ - \theta_-)}^{\frac{1}{2}(\theta_- - \theta_+)} \frac{\hat{n}(\psi)}{\sqrt{\sin(\psi + \frac{1}{2}(\theta_- - \theta_+)) \sin(\frac{1}{2}(\theta_- - \theta_+) - \psi)}} d\psi. \quad (27)$$

The unit vector $\hat{n}(\psi)$ points from the infinitesimal charge on the segment to the observation point, with angle $\theta = \psi + \frac{1}{2}(\theta_+ + \theta_-)$ measured from the x -axis in the usual counterclockwise sense on the xy -plane. Thus $\cos \theta = \hat{x} \cdot \hat{n}(\psi)$. Correspondingly, θ_{\pm} are the angles from the ends of the line segment to the observation point, as given by $\cos \theta_{\pm} = \hat{x} \cdot \hat{r}_{\pm}$. Since the integration over ψ weights $\hat{n}(\psi)$ by an *even* function of ψ , and the range of integration is *symmetric* about $\psi = 0$, it follows that the resulting direction of $\vec{E}(x, y)$ will be proportional to $\hat{n}(\psi = 0) = (\hat{r}_+ + \hat{r}_-) / |\hat{r}_+ + \hat{r}_-|$ which points in direction $\frac{1}{2}(\theta_+ + \theta_-)$. That is to say,

$$\hat{x} \cdot \vec{E}(x, y) = |\vec{E}(x, y)| \cos\left(\frac{\theta_+ + \theta_-}{2}\right), \quad \hat{y} \cdot \vec{E}(x, y) = |\vec{E}(x, y)| \sin\left(\frac{\theta_+ + \theta_-}{2}\right). \quad (28)$$

The change of variables needed to obtain (27) will be discussed more fully below, for non-uniformly charged segments giving rise to ellipsoidal equipotentials in any number of dimensions.

A direct graphical comparison of the uniformly charged segment and the non-uniformly charged segment in 2D is obtained by superimposing their equipotentials in a true orthogonal projection of the Φ surface contours onto the xy -plane.

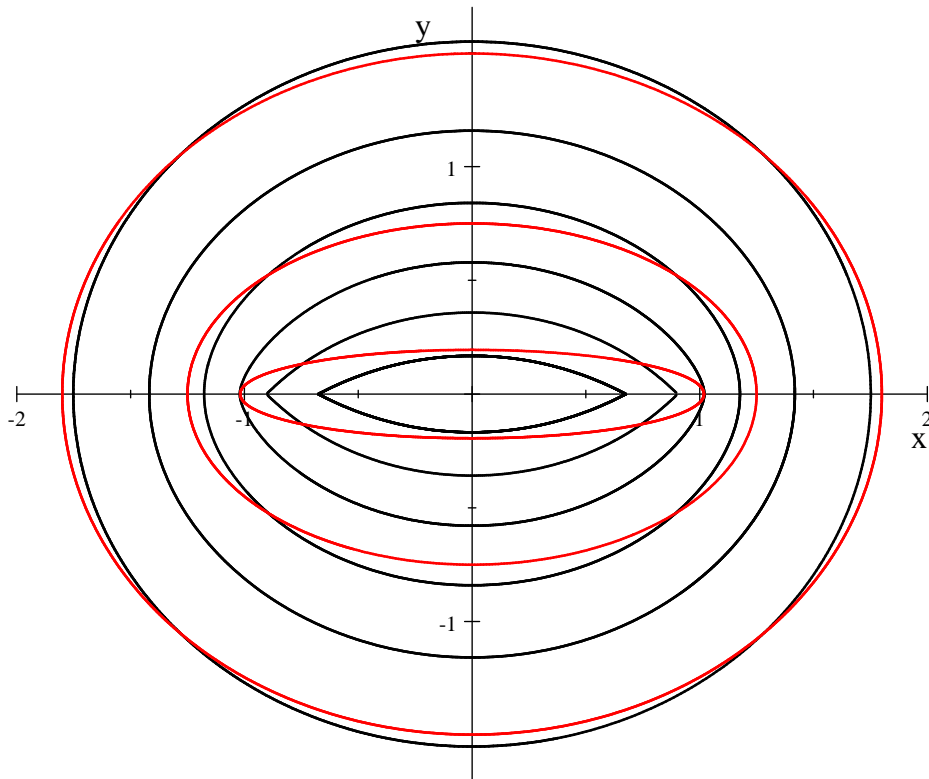


Figure 13: 2D equipotential contours for a uniformly charged segment, with constant λ for $-1 \leq x \leq 1$, for $\Phi = 1.5, 1.0, 0.5, 0.0, -0.5$, and -1.0 , as inner to outer black curves, and ellipsoidal contours for a coincident non-uniformly charged segment, for $\Phi = 1.0, 0.0$, and -1.0 , as inner to outer red curves.

For large distances from the line segments, whether uniformly charged or otherwise, the potential approaches that of a point charge as given in (1). So asymptotically both sets of contours become circles. Regarding this, recall the total charge on either segment under consideration is the same, namely, $Q = \lambda L$. Thus for large distances from the segment the equipotentials in Figure 13 will coalesce, although it is perhaps surprising how rapidly this occurs. In Figure 13 the equipotential contours for both the uniform and non-uniform charge distributions, for the same value of Φ , are very nearly coincident if $r \gtrsim 2L$ — the exact locations of the two sets of contours never differ by more than a few percent if $r \gtrsim 2L$ — well before the contours reach their asymptotic circular form.

3 Point charge in D dimensions

For a point charge Q located at the origin of coordinates, in $D > 2$ dimensions, the scalar potential at an observation point \vec{r} is hypothesized to be [15]

$$\Phi_{\text{point}}(D, \vec{r}) = \frac{kQ}{r^{D-2}}, \quad (29)$$

where k is the D -dimensional analogue of Coulomb's constant. Integrating the radial gradient of Φ_{point} over the surface of a sphere fixes the normalization, by Gauss' law.

$$\vec{E}_{\text{point}}(\vec{r}) = -\vec{\nabla}\Phi_{\text{point}}(D, \vec{r}) = -\hat{r} \partial_r \Phi_{\text{point}}(D, \vec{r}) = \frac{(D-2)kQ \hat{r}}{r^{D-1}}, \quad (30)$$

$$\int_{r \leq R} \vec{\nabla} \cdot \vec{E}(\vec{r}) d^D r = \int_{S_{D-1}} \vec{E}(R\hat{r}) \cdot \hat{r} R^{D-1} d\Omega = (D-2)\Omega_D kQ, \quad (31)$$

where the total solid angle (i.e. the area of the *unit radius* sphere, S_{D-1} , embedded in D dimensions) is given by

$$\Omega_D = \int_{S_{D-1}} d\Omega = \frac{2\pi^{D/2}}{\Gamma(D/2)}. \quad (32)$$

For example, $\Omega_1 = 2$, $\Omega_2 = 2\pi$, $\Omega_3 = 4\pi$, $\Omega_4 = 2\pi^2$, etc.

To put it differently, in terms of a Dirac delta in D -dimensions,

$$\vec{\nabla} \cdot \vec{E}_{\text{point}}(\vec{r}) = (D-2)\Omega_D kQ \delta^D(\vec{r}), \quad (33)$$

$$\nabla^2 \left(\frac{1}{r^{D-2}} \right) = -(D-2)\Omega_D \delta^D(\vec{r}). \quad (34)$$

And in fact, this gives the correct result even for $D = 2$, by taking a limit:

$\nabla^2 \left(1 - (D-2) \ln r + O((D-2)^2) \right) \underset{D \rightarrow 2}{\sim} -(D-2)\Omega_2 \delta^2(\vec{r})$, hence $\nabla^2 \ln r = 2\pi \delta^2(\vec{r})$. So for $D = 2$ the point particle potential is logarithmic, as previously noted in Section 2.

Perhaps the simplest convention would be to set

$$Q = \int \vec{E}(\vec{r}) \cdot \hat{r} r^{D-1} d\Omega, \quad \nabla^2 \Phi_{\text{point}}(D, \vec{r}) = -Q \delta^D(\vec{r}),$$

which would require, for $D > 2$,

$$k = \frac{1}{(D-2)\Omega_D} = \frac{\Gamma(D/2)}{(D-2)2\pi^{D/2}}.$$

This is singular at $D = 2$ where the potential is a logarithm, not a power. In that case the corresponding choice would be $k = \frac{1}{2\pi}$, so

$$\Phi_{\text{point}}(D = 2, \vec{r}) = -\frac{Q}{2\pi} \ln r,$$

and again $\nabla^2 \Phi_{\text{point}}(D = 2, \vec{r}) = -Q \delta^2(\vec{r})$.

4 Uniformly charged line segments for all dimensions $D > 2$

The line of charge and observation point are shown in red in the following Figure.

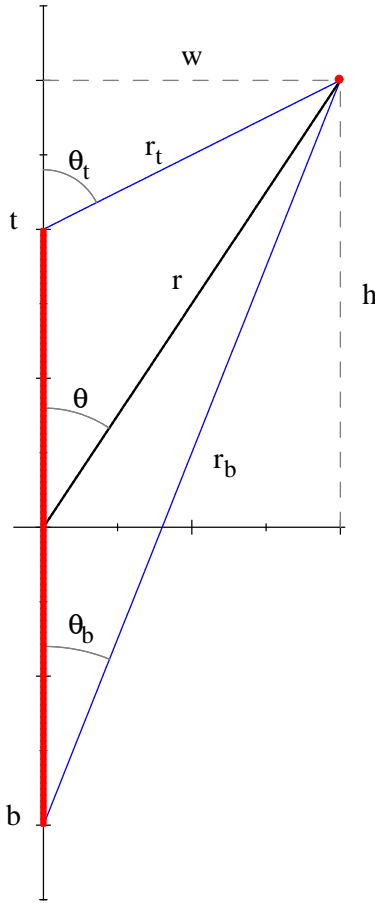


Figure 14: Segment coordinates.

From the Figure (+ and - in the formulas correspond, respectively, to the bottom point “b” and the top point “t” in the Figure)

$$r_t = \sqrt{\frac{1}{4}L^2 - Lr \cos \theta + r^2}, \quad r_b = \sqrt{\frac{1}{4}L^2 + Lr \cos \theta + r^2}, \quad (35a)$$

$$\sin \theta_{b,t} = \frac{r \sin \theta}{\sqrt{\frac{1}{4}L^2 \pm Lr \cos \theta + r^2}}, \quad \cos \theta_{b,t} = \frac{r \cos \theta \pm L/2}{\sqrt{\frac{1}{4}L^2 \pm Lr \cos \theta + r^2}}, \quad (35b)$$

$$\frac{\sin \theta_b}{r_t} = \frac{\sin \theta_t}{r_b} = \frac{\sin(\theta_t - \theta_b)}{L}, \quad (35c)$$

$$\theta_t - \theta_b = \arcsin \left(\frac{Lr \sin \theta}{\sqrt{\left(\frac{1}{4}L^2 + r^2\right)^2 - L^2 r^2 \cos^2 \theta}} \right). \quad (35d)$$

The relations in the third line above follow from the Law of Sines. Note that the last expression must be used with care since arcsin is multi-valued. In particular, if $r < L/2$, then as the segment is approached it is always true that $\theta_t - \theta_b \rightarrow \pi$, no matter how the segment is approached.

More generally, when r decreases to cross the surface of the sphere for which the segment is a diameter, the value of arcsin increases through $\pi/2$. This follows from $\left. \sqrt{\left(\frac{1}{4}L^2 + r^2\right)^2 - L^2 r^2 \cos^2 \theta} \right|_{r=L/2} = \frac{1}{2}L^2 \sin \theta$

so that the argument of the arcsin in (35d) is just 1 for $r = L/2$, and $\theta_t - \theta_b = \pi/2$ at this radius. Reducing r below $L/2$ increases $\theta_t - \theta_b$ above $\pi/2$, i.e. arcsin has moved onto another branch of the function. This change of branch can be explicitly taken into account through the use of Heaviside step functions, Θ , to write

$$\theta_t - \theta_b = \pi \Theta\left(\frac{L}{2} - r\right) + \left(\Theta\left(r - \frac{L}{2}\right) - \Theta\left(\frac{L}{2} - r\right)\right) \arcsin\left(\frac{Lr \sin \theta}{\sqrt{\left(\frac{1}{4}L^2 + r^2\right)^2 - L^2 r^2 \cos^2 \theta}}\right), \quad (36)$$

where the arcsin in this expression is the principal branch of the function.

Assuming linear superposition for the potential, a uniformly charged line segment as shown above in Figure 14, of length L , centered on the origin, with top (t) and bottom (b) ends at $\theta = 0$ (i.e. $z = L/2$) and $\theta = \pi$ (i.e. $z = -L/2$), will produce in $D > 2$ dimensions a potential Φ_{line} given by [16]

$$\Phi_{\text{line}}(D, r, \theta) = \frac{k\lambda}{(r \sin \theta)^{D-3}} \int_{\theta_b}^{\theta_t} (\sin \vartheta)^{D-4} d\vartheta. \quad (37)$$

Here λ is the constant charge/length on the line segment, and $\theta_{t,b}$ are the polar angles for vectors from the top and bottom endpoints of the line segment to the observation point (r, θ) , as in Figure 14.

The potential has no dependence on the additional $D - 2$ angles needed to specify the location of a point in D dimensions using spherical polar coordinates. That is to say, in D dimensions the equipotentials are always higher dimensional surfaces of revolution about the line segment. The corresponding electric field is given by

$$\vec{E}_{\text{line}}(\vec{r}) = -\vec{\nabla} \Phi_{\text{line}} = -\hat{r} \partial_r \Phi_{\text{line}} - \frac{1}{r} \hat{\theta} \partial_\theta \Phi_{\text{line}}, \quad (38)$$

and it depends manifestly on r and θ . The only dependence of the electric field on the additional $D - 2$ angles in D dimensional spherical polar coordinates is carried by the unit vectors \hat{r} and $\hat{\theta}$.

To see that (37) is correct, we need only sum the potential contributions for infinitesimal pieces of the line segment with charge

$$dQ = \lambda dz, \quad (39)$$

located on the vertical axis of Figure 14 at position z , and at a distance $\ell(z)$ from the observation point (r, θ) as given by

$$\ell(z) = \sqrt{r^2 + z^2 - 2rz \cos \theta}. \quad (40)$$

But writing $z = h - w \cot \vartheta$ and $\ell(z) = \frac{w}{\sin \vartheta}$, for fixed h and w , we have $dz = -w d \cot \vartheta = \frac{w}{\sin^2 \vartheta} d\vartheta$, and

$$\int_{-L/2}^{L/2} \frac{dz}{(\ell(z))^{D-2}} = \frac{1}{w^{D-3}} \int_{\theta_b}^{\theta_t} (\sin \vartheta)^{D-4} d\vartheta. \quad (41)$$

On the other hand, $w = r \sin \theta$. Hence the result (37).

For instance, in the special case $D = 3$ the potential of the uniformly charged segment is

$$\Phi_{\text{line}}(D = 3, r, \theta) = k\lambda \int_{\theta_b}^{\theta_t} \frac{1}{\sin \vartheta} d\vartheta = k\lambda \ln \left(\frac{\sin \vartheta}{1 + \cos \vartheta} \right) \Big|_{\vartheta=\theta_b}^{\vartheta=\theta_t}. \quad (42)$$

Note that the potential is infinite for all points on the charged segment itself, for which points $\theta_b = 0$ and $\theta_t = \pi$. Be that as it may, after a bit of algebra $\Phi_{\text{line}}(D = 3)$ can be reduced to

$$\Phi_{\text{line}}(D = 3, r, \theta) = k\lambda \ln \left(\frac{s + L}{s - L} \right), \quad (43)$$

where

$$s = r_t + r_b \quad (44)$$

is the sum of the distances from the end points of the segment to the observation point. Thus equipotentials in this case are given by constant s , and as is common knowledge, this defines an ellipsoid of revolution about the line segment with focal points t and b . A view from below the potential surface again clearly shows the equipotentials are ellipses.

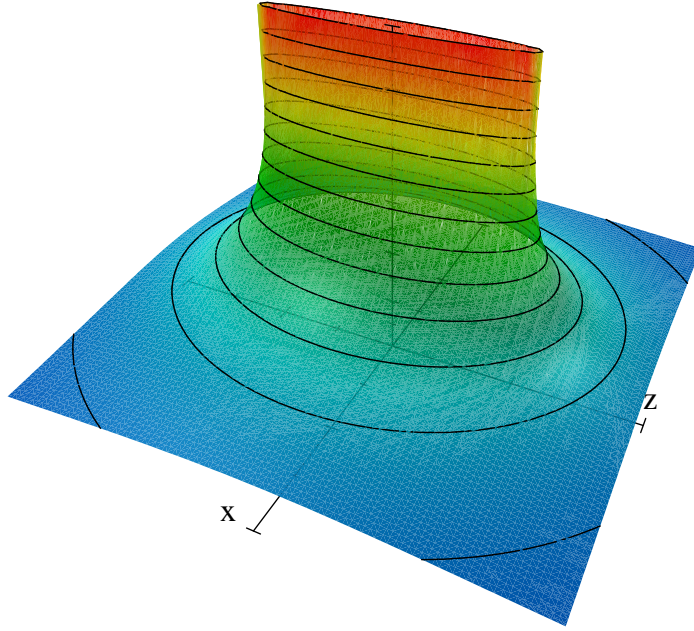


Figure 15: $\frac{1}{k\lambda} \Phi_{\text{line}}(D=3, r, \theta) = \ln \left(\frac{\sqrt{1-2z+r^2} + \sqrt{1+2z+r^2} + 2}{\sqrt{1-2z+r^2} + \sqrt{1+2z+r^2} - 2} \right)$ for $L=2$, where $z = r \cos \theta$ and $x = r \sin \theta$.

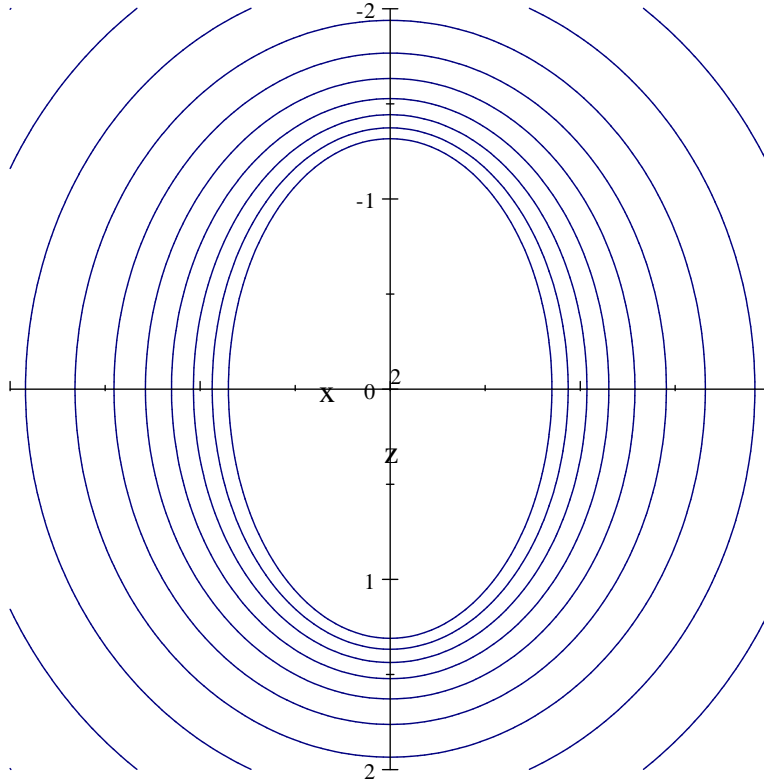


Figure 16: Contours of constant $\frac{1}{k\lambda} \Phi_{\text{line}}(D=3, r, \theta) = \ln \left(\frac{\sqrt{1-2z+r^2} + \sqrt{1+2z+r^2} + 2}{\sqrt{1-2z+r^2} + \sqrt{1+2z+r^2} - 2} \right)$ for $L=2$, plotted versus $z = r \cos \theta$ (vertical axis) and $x = r \sin \theta$ (horizontal axis).

For other dimensions, however, the geometrical shapes of the equipotentials are not so easily discerned. For $D > 3$, it remains to evaluate the angular integral in (37). Define the indefinite integral $I(D) = \int (\sin \vartheta)^{D-4} d\vartheta$, and compute

$$\begin{aligned}
 I(4) &= \vartheta, & I(5) &= -\cos \vartheta, \\
 I(6) &= \frac{1}{2}\vartheta - \frac{1}{2}\cos \vartheta \sin \vartheta, & I(7) &= \frac{1}{3}\cos^3 \vartheta - \cos \vartheta, \\
 I(8) &= \frac{3}{8}\vartheta + \left(\frac{1}{4}\cos^3 \vartheta - \frac{5}{8}\cos \vartheta\right) \sin \vartheta, & I(9) &= -\frac{1}{5}\cos^5 \vartheta + \frac{2}{3}\cos^3 \vartheta - \cos \vartheta,
 \end{aligned} \tag{45}$$

etc. For odd $D \geq 5$ the integral is always a polynomial of order $D - 4$ in $\cos \vartheta$, while for even $D \geq 4$ the integral always has a term linear in ϑ plus, for $D \geq 6$, a term with $\sin \vartheta$ multiplying a polynomial of order $D - 5$ in $\cos \vartheta$. For any D we therefore obtain the angular integral in (37) in terms of $(\theta_t - \theta_b)$, $\sin \theta_t$, $\sin \theta_b$, $\cos \theta_t$, and $\cos \theta_b$. These quantities may then be expressed in terms of θ and r upon using the relations in (35a-35d).

For example, in $D = 4$ the potential of the uniformly charged segment is

$$\Phi_{\text{line}}(D = 4, r, \theta) = \frac{k\lambda}{r \sin \theta} (\theta_t - \theta_b). \tag{46}$$

Unlike $\Phi_{\text{line}}(D = 3)$, the potential $\Phi_{\text{line}}(D = 4)$ is *not* a function solely of the variable s as defined in (44). Consequently, the equipotentials are *not* ellipsoidal for this four dimensional example. Indeed, a plot now shows that the equipotentials are not ellipsoidal, especially for points close to the uniform line of charge, although the shape of the potential surface is similar to that for $D = 3$.

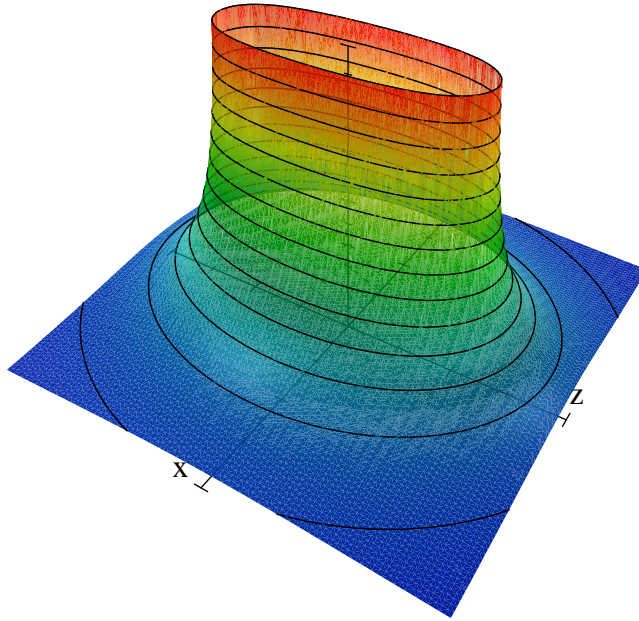


Figure 17: $\frac{1}{k\lambda} \Phi_{\text{line}}(D = 4, r, \theta) = \frac{1}{|x|} \arcsin\left(\frac{2|x|}{\sqrt{(1+r^2)^2 - 4z^2}}\right)$ for $L = 2$, where $z = r \cos \theta$ and $x = r \sin \theta$.

Note that Φ_{line} is infinite for all points on the segment. Also note, to obtain the correct shape of the potential surface it is important to interpret \arcsin in the formula for Φ_{line} as a multi-valued function, as given explicitly by (36).

A view from below the potential surface shows that the potential contours are *not* ellipses in this case, although the difference is somewhat subtle. This next graph should be compared closely to the ellipsoidal case for $D = 4$ as presented below in Section 5.

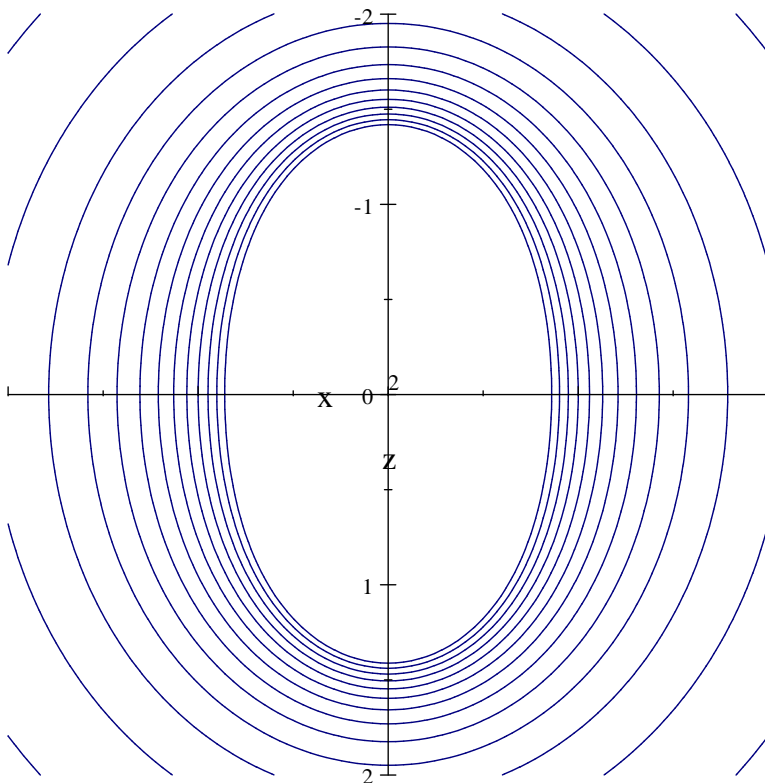


Figure 18: Contours of constant $\frac{1}{k\lambda} \Phi_{\text{line}}(D = 4, r, \theta) = \frac{1}{|x|} \arcsin\left(\frac{2|x|}{\sqrt{(1+r^2)^2 - 4z^2}}\right)$ for $L = 2$.

The electric field is given by (38) and in this case has r and θ components

$$-\partial_r \Phi_{\text{line}}(D = 4) = -\frac{k\lambda}{r \sin \theta} \partial_r (\theta_t - \theta_b) + \frac{1}{r} \Phi_{\text{line}}(D = 4) , \quad (47)$$

$$-\frac{1}{r} \partial_\theta \Phi_{\text{line}}(D = 4) = -\frac{k\lambda}{r^2 \sin \theta} \partial_\theta (\theta_t - \theta_b) + \frac{\cot \theta}{r} \Phi_{\text{line}}(D = 4) . \quad (48)$$

All the complication in these expressions lies in the derivatives $\partial_r (\theta_t - \theta_b)$ and $\partial_\theta (\theta_t - \theta_b)$ whose geometrical significance is not yet easy to visualize. On the other hand, the last terms involving $\frac{1}{r} \Phi_{\text{line}}$ in (47) and (48) have simple geometrical interpretations since they define a vector that is perpendicular to the axis of the segment and points away from that axis for positive λ (i.e. in the direction of $\hat{\rho} = \hat{r} \sin \theta + \hat{\theta} \cos \theta$ if we were to use cylindrical coordinates).

In any case, it is worthwhile to compute $\partial_r (\theta_t - \theta_b)$ and $\partial_\theta (\theta_t - \theta_b)$ since these derivatives appear for all even $D \geq 4$ and always have the same form. After some algebra we find

$$\partial_r (\theta_t - \theta_b) = \frac{4(L^2 + 4r^2)L \sin \theta}{(L^2 + 4r^2)^2 - 16L^2 r^2 \cos^2 \theta} \operatorname{sgn}(L^2 - 4r^2) , \quad (49)$$

$$\frac{1}{r} \partial_\theta (\theta_t - \theta_b) = \frac{4(L^2 - 4r^2)L \cos \theta}{(L^2 + 4r^2)^2 - 16L^2 r^2 \cos^2 \theta} \operatorname{sgn}(L^2 - 4r^2) . \quad (50)$$

Note the difference in sign for $r^2 \geq \frac{1}{4}L^2$. Once again $\hat{\rho} = \hat{r} \sin \theta + \hat{\theta} \cos \theta$, so the bulk of the contributions from these derivatives again gives a vector that is perpendicular to the axis of the segment. But there

remains a contribution that is entirely in the \hat{r} direction if $L^2 + 4r^2$ is written as $L^2 - 4r^2 + 8r^2$, or else entirely in the $\hat{\theta}$ direction if $L^2 - 4r^2$ is written as $L^2 + 4r^2 - 8r^2$. Choosing the first of these options gives

$$\begin{aligned} \vec{E}_{\text{line}}(D=4, \vec{r}) &= \left(\frac{1}{r} \Phi_{\text{line}}(D=4, r, \theta) - \frac{4Lk\lambda}{r} \frac{|L^2 - 4r^2|}{(L^2 + 4r^2)^2 - 16L^2r^2 \cos^2 \theta} \right) (\hat{r} + \hat{\theta} \cot \theta) \\ &\quad - \left(\frac{32k\lambda r L}{(L^2 + 4r^2)^2 - 16L^2r^2 \cos^2 \theta} \operatorname{sgn}(L^2 - 4r^2) \right) \hat{r} \end{aligned} \quad (51)$$

To compare to the three dimensional ellipsoidal case, it suffices to express \hat{r} and $\hat{\theta}$ in terms of \hat{r}_t and \hat{r}_b . Although the latter two unit vectors are not orthogonal, they are independent except at $\theta = 0$ and $\theta = \pi$, and at those particular angles either one of \hat{r}_t and \hat{r}_b will suffice to give the direction of the electric field, since \vec{E}_{line} (on the z -axis) $\propto \hat{z}$. We find

$$\begin{aligned} \hat{r} &= \frac{1}{2r} (\vec{r}_t + \vec{r}_b) \\ &= \left(\frac{1}{4r} \sqrt{L^2 - 4Lr \cos \theta + 4r^2} \right) \hat{r}_t + \left(\frac{1}{4r} \sqrt{L^2 + 4Lr \cos \theta + 4r^2} \right) \hat{r}_b, \end{aligned} \quad (52)$$

$$\begin{aligned} \hat{\theta} &= \frac{1}{Lr^2 \sin \theta} ((\vec{r} \cdot \vec{r}_b) \vec{r}_t - (\vec{r} \cdot \vec{r}_t) \vec{r}_b) \\ &= \frac{2r + L \cos \theta}{4Lr \sin \theta} \sqrt{L^2 - 4Lr \cos \theta + 4r^2} \hat{r}_t - \frac{2r - L \cos \theta}{4Lr \sin \theta} \sqrt{L^2 + 4Lr \cos \theta + 4r^2} \hat{r}_b. \end{aligned} \quad (53)$$

5 Ellipsoidal equipotentials for all dimensions $D > 2$

Consider the same geometry as in Figure 14, but rather than assuming uniform charge density on the line segment, suppose the potential produced by the line segment depends positionally only on s in any number of dimensions. Including some convenient numerical and dimensionful factors, suppose

$$\Phi(\vec{r}) = k\lambda L \left(\frac{2}{L} \right)^{D-2} V(s), \quad s = r_t + r_b. \quad (54)$$

In this case, equipotentials are ellipsoidal by assumption, since the positional dependence is only on s . The only issue is to determine $V(s)$.

If the only charge present is on the line segment, then for other points the potential function must be harmonic, $\nabla^2 \Phi(\vec{r}) = 0$. So, using $\vec{\nabla} r_t = \vec{r}_t / r_t$ and $\vec{\nabla} r_b = \vec{r}_b / r_b$ (see Eqns(5)-(7) in [11] for more details), we compute

$$\nabla^2 V(s) = \frac{1}{r_t r_b} ((D-1) s V'(s) + (s^2 - L^2) V''(s)). \quad (55)$$

The potential will then be harmonic for points not lying on the segment if and only if

$$(L^2 - s^2) V''(s) + (1 - D) s V'(s) = 0 \quad (56)$$

for $s > L$. For general D the relevant solution of this second order, ordinary differential equation, is given by a Gauss hypergeometric function represented by the standard series around $s = \infty$, namely,

$$V(s) = \left(\frac{s}{L} \right)^{2-D} {}_2F_1 \left(\frac{1}{2}D - 1, \frac{1}{2}D - \frac{1}{2}; \frac{1}{2}D; L^2/s^2 \right), \quad (57)$$

$$\underset{s \rightarrow \infty}{\sim} \left(\frac{L}{s} \right)^{D-2} + O \left(\frac{L^D}{s^D} \right) \quad \text{for } D > 2, \quad (58)$$

$$\underset{s \rightarrow L}{\sim} \frac{D-2}{D-3} \left(\sqrt{\frac{L/2}{s-L}} \right)^{D-3} \quad \text{for } D > 3, \quad (59)$$

The various factors in the last line are useful to determine the exact expression for the charge distribution along the segment, as presented below (see (67)). Note the large s behavior of V implies

$$\Phi(\vec{r}') \underset{r \rightarrow \infty}{\sim} \frac{k\lambda L}{r^{D-2}} + O\left(\frac{1}{r^D}\right) \quad (60)$$

since $s \underset{r \rightarrow \infty}{\sim} 2r$. The normalization of V and the $2/L$ factors in (54) were chosen so that the total charge on the segment is the same as in the uniformly charged case, namely, $Q = \lambda L$. This total charge appears in the limiting form of the potential for $r \gg L$, i.e. $\lim_{r \rightarrow \infty} r^{D-2} \Phi(\vec{r}') / k = Q$.

Alternatively, closed-form expressions for $V(s)$ in terms of more elementary functions are sometimes more easily obtained by evaluating the corresponding hypergeometric series around $s = 0$, as given by [17]

$$V(s) = A(D) \frac{s}{L} {}_2F_1\left(\frac{1}{2}, \frac{1}{2}D - \frac{1}{2}; \frac{3}{2}; s^2/L^2\right) + B(D) , \quad (61)$$

and then analytically continuing to $s > L$. Here $A(D)$ and $B(D)$ are constants chosen so that the result (61) is real-valued for $s > L$, and so that any constant term (the trivial harmonic) is eliminated from V as $s \rightarrow \infty$.

For integer D the hypergeometric functions that appear in the solutions (57) and (61) always reduce to elementary functions. For example, in various dimensions the relevant harmonic functions are:

$$D = 1 , \quad V(s) = s/L \quad (62)$$

$$D = 2 , \quad V(s) = \ln\left(\frac{2L}{s + \sqrt{s^2 - L^2}}\right) \quad (63)$$

$$\underset{s \rightarrow \infty}{\sim} \ln\left(\frac{L}{s}\right) + O\left(\frac{L^2}{s^2}\right)$$

$$D = 3 , \quad V(s) = \frac{1}{2} \ln\left(\frac{s+L}{s-L}\right) \quad (64)$$

$$\underset{s \rightarrow \infty}{\sim} \frac{L}{s} + O\left(\frac{L^3}{s^3}\right)$$

$$D = 4 , \quad V(s) = 2\left(\frac{s}{\sqrt{s^2 - L^2}} - 1\right) \quad (65)$$

$$\underset{s \rightarrow \infty}{\sim} \frac{L^2}{s^2} + O\left(\frac{L^4}{s^4}\right)$$

$$D = 5 , \quad V(s) = -\frac{3}{4} \left(\ln\left(\frac{s+L}{s-L}\right) - \frac{2sL}{s^2 - L^2} \right) \quad (66)$$

$$\underset{s \rightarrow \infty}{\sim} \frac{L^3}{s^3} + O\left(\frac{L^5}{s^5}\right)$$

By construction, the equipotentials are always ellipsoidal for any D , except for the trivial one dimensional case where equipotentials consist of just pairs of points on the line. In contrast to the uniformly charged line segment for $D \neq 3$, if the potential depends only on s then the charged line itself — where $s = L$ for all points on the segment — is *always* an equipotential, albeit with *infinite* Φ when $D \geq 3$, while for $D = 1$ and $D = 2$ the potential along the charged line is *finite*.

For example, consider graphically the case for $D = 4$. Qualitatively the potential surface is similar to that for the uniformly charged segment in three dimensions. Potential contours are ellipsoids that surround $-L/2 \leq z \leq L/2$ and *never* intersect the charge segment. Also, the top of the potential surface is just an exact copy of the segment itself, albeit at an infinite value of Φ . That is to say, the charged segment is itself an equipotential, but in fact the potential is infinite for points on the segment. Again, a view from below the potential surface shows more clearly the ellipsoidal potential contours.

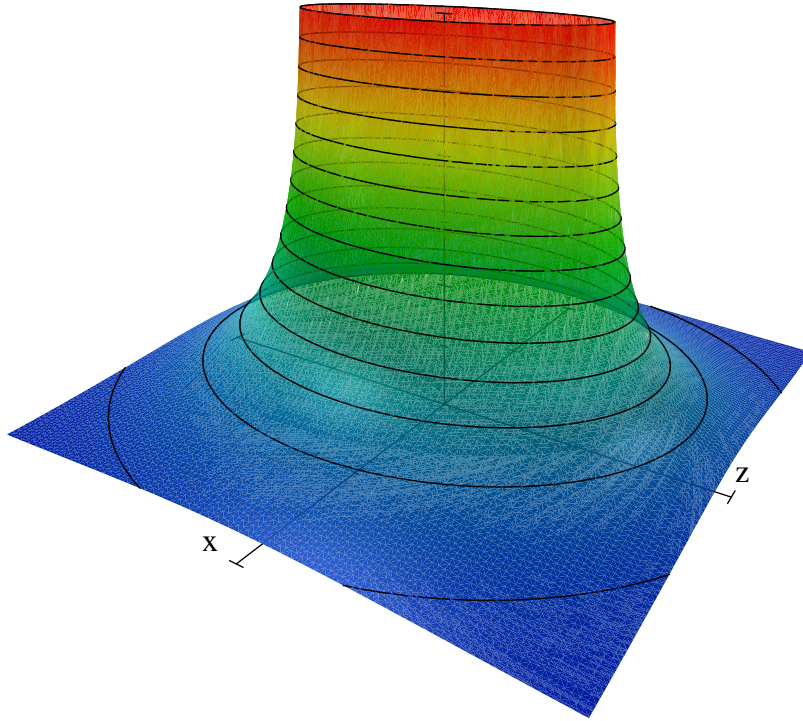


Figure 19: $\frac{1}{k\lambda} \Phi = L \left(\frac{2}{L}\right)^{D-2} V(s) \Big|_{D=4} = \frac{8}{L} \left(\frac{s}{\sqrt{s^2-L^2}} - 1\right)$ for $L = 2$, versus $z = r \cos \theta$ and $x = r \sin \theta$.

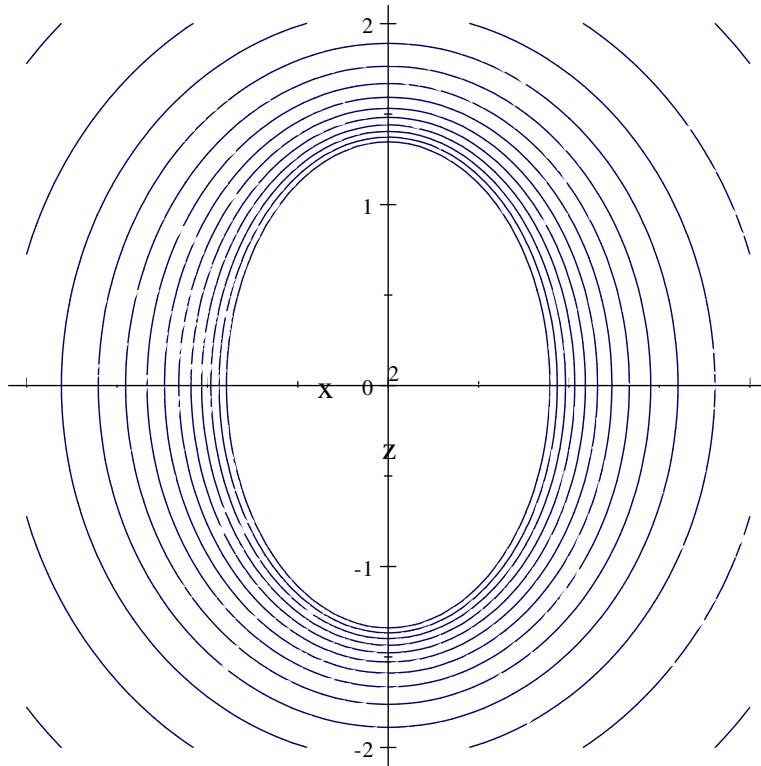


Figure 20: Contours of constant $\frac{1}{k\lambda} \Phi = L \left(\frac{2}{L}\right)^{D-2} V(s) \Big|_{D=4} = \frac{8}{L} \left(\frac{s}{\sqrt{s^2-L^2}} - 1\right)$ for $L = 2$.

Admittedly, in 4D it takes a discerning eye to see differences in the shape of the ellipsoidal equipotential surface compared to that for the uniformly charged segment, if graphs of the two cases are viewed separately. But if viewed side-by-side the difference *is* evident in contour plots for the potentials. Perhaps even more clearly, the difference is highlighted by plotting both cases in the same graph.

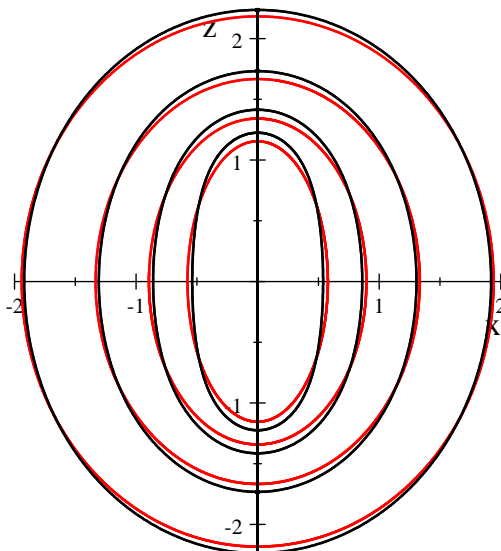


Figure 21: Comparison of Φ contours in 4D for a uniformly charged segment (black) and a non-uniformly charged segment with ellipsoidal equipotentials (red) for $L = 2$.

Upon doing so, it is also evident that the non-uniform charge distribution must be greater near the center of the segment rather than at the ends of the segment, a counter-intuitive feature. The ellipsoidal equipotentials are shorter in the direction of the line segment, and wider transverse to the segment, than those of the uniformly charged line for the same value of Φ . This is exactly the opposite of what happens in 2D, where the ellipsoidal equipotentials were longer and narrower than those of the uniformly charged segment for the same value of Φ .

The non-uniform charge distribution on the segment that produces ellipsoidal equipotentials can now be determined using the integral form of Gauss' Law in D dimensions, (31), in complete parallel to the calculation leading to (26) in 2D. Here we only give the results of that calculation.

In D dimensions the charge density for a line segment that produces ellipsoidal equipotentials is

$$\lambda_D(z) = 2\lambda \frac{\Omega_{D-1}}{\Omega_D} \left(\sqrt{1 - \frac{4z^2}{L^2}} \right)^{D-3}, \quad (67)$$

where we have used the ratio of total "solid angles" in D and $D - 1$ dimensions,

$$\frac{\Omega_{D-1}}{\Omega_D} = \frac{\Gamma(\frac{1}{2}D)}{\sqrt{\pi}\Gamma(\frac{1}{2}D - \frac{1}{2})}. \quad (68)$$

For example, $\left. \frac{\Gamma(\frac{1}{2}D)}{\sqrt{\pi}\Gamma(\frac{1}{2}D - \frac{1}{2})} \right|_{D=2} = \frac{1}{\pi}$ to give $\lambda_{D=2}(z)$ in agreement with (10), while $\left. \frac{\Gamma(\frac{1}{2}D)}{\sqrt{\pi}\Gamma(\frac{1}{2}D - \frac{1}{2})} \right|_{D=3} = \frac{1}{2}$ to give the uniform distribution, $\lambda_{D=3}(z) = \lambda$. These charge densities are all normalized so that the total charge on the segment is the same for any D , namely,

$$Q = \lambda L = \int_{-L/2}^{L/2} \lambda_D(z) dz. \quad (69)$$

This follows from

$$\int_{-L/2}^{L/2} \lambda_D(z) dz = \lambda L \frac{\Omega_{D-1}}{\Omega_D} \int_{-1}^1 (1-u^2)^{\frac{D-3}{2}} du, \quad (70)$$

$$\int_{-1}^1 (1-u^2)^{\frac{D-3}{2}} du = \frac{\sqrt{\pi} \Gamma(\frac{1}{2}D - \frac{1}{2})}{\Gamma(\frac{1}{2}D)} = \frac{\Omega_D}{\Omega_{D-1}}. \quad (71)$$

A geometrical construction to obtain the distribution (67) is to consider a uniformly charged S_{D-1} , i.e. a hypersphere embedded in D dimensions, with radius $R = L/2$ and with *constant* hypersurface charge density $\sigma_D = Q/(\Omega_D R^{D-1})$. An orthogonal projection of the charge, dQ , from a hyper-cylindrical “ribbon” of revolution about a diameter of the hypersphere onto the underlying surrounded segment dz of the diameter, gives precisely $dQ/dz = \lambda_D(z)$ for $-L/2 \leq z \leq L/2$. This follows directly from $dQ = \sigma_D dA$, where the hypersurface “area” dA of the hyper-ribbon that surrounds dz is $dA = \Omega_{D-1} R^{D-2} \sin^{D-2} \theta ds$ with $ds = R d\theta$, $z = R \cos \theta$, and $\sin \theta = \sqrt{1 - z^2/R^2}$. This construction is easily visualized for $D = 2$ and 3.

We plot the densities for various integer D , from $D = 2$ up to $D = 11$, shown respectively as the lower to upper curves (for $z = 0$) in the following graph.

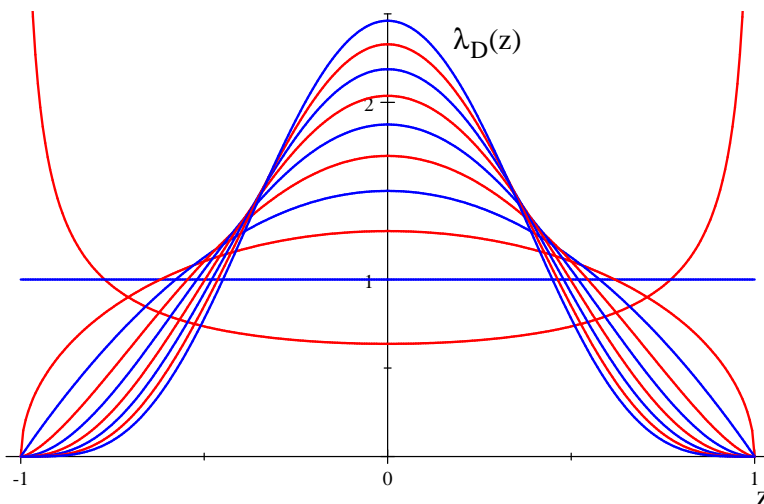


Figure 22: Linear charge density $\lambda_D(z)$ leading to ellipsoidal equipotentials, in various dimensions.

In this graph the 2D case is the only one which is intuitive in the sense that the infinitesimal pieces of charge repel each other so we would expect excess charge/length to be pushed towards the ends of a finite length, equipotential segment of real conductor with small but nonzero transverse size, all parts of which are at the same finite Φ . For the idealized line segment in 3D this is not so — the charge density is uniform — but then the segment itself is at an infinite Φ so physical intuition based on real conductors is perhaps difficult to apply in this situation [18]. In higher dimensions, the result is even *more* counter-intuitive for idealized line segments. The charge distribution is peaked at the center of the segment. Of course, in making these statements, we are assuming the physical properties of the idealized segment itself can be completely understood mathematically by taking the limit of the surrounding equipotential ellipsoids of revolution as their girth goes to zero.

To gain more insight about the behavior of the charge distribution and the resulting potential, we may think of D in (67) as a continuous variable — not just an integer — to be used as a regulating parameter by which the $D = 3$ case can be approached as a limit. This point of view shows that all $D < 3$ behave intuitively, with $\lambda_D(z)$ peaked at the ends of the segment. The extreme case is $D = 1$ where all charge is located *only* at the ends of the segment. Moreover, for all $D < 3$ the potential along the segment, as given by (57), is a *finite* constant, so there is nothing pathological about the potential that might obviate physical intuition based on real conductors.

On the other hand, all $D > 3$ behave counter-intuitively, with $\lambda_D(z)$ peaked at the center of the segment and vanishing at the segment ends. And for all $D > 3$ the potential along the segment, as given by (57), is

infinite, so real-world physical intuition is not guaranteed to be reliable for these idealized situations. The uniformly charged 3D case, also with infinite Φ along the segment, acts as a separatrix between intuitive and counter-intuitive charge distributions. A plot of $\lambda_D(z)$ as a surface over the (z, D) plane helps to visualize these features.

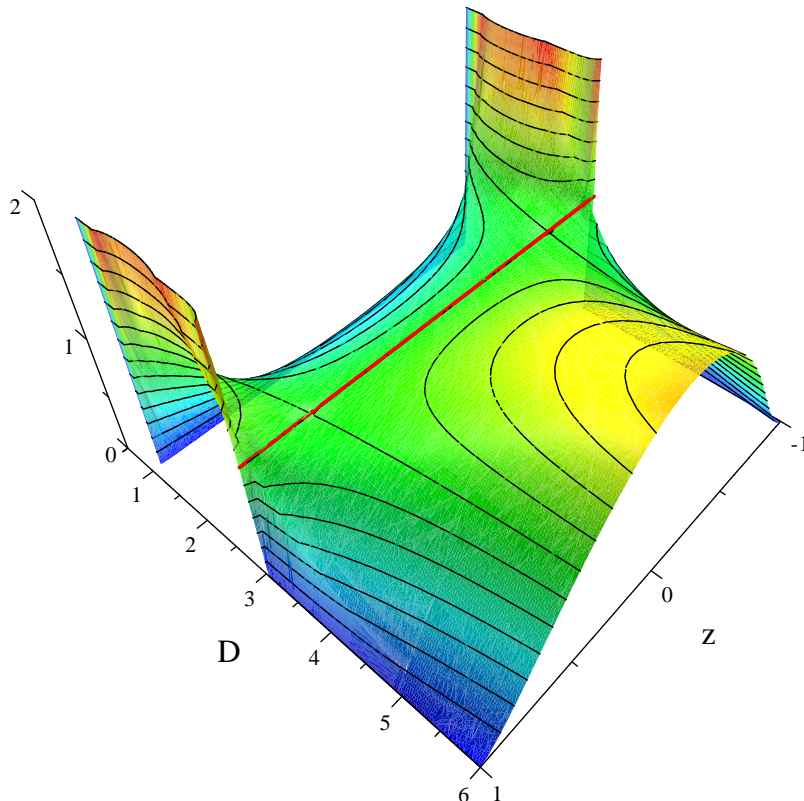


Figure 23: The $\lambda_D(z)$ surface as a continuous function of both z and D for a straight-line segment from $z = -1$ to $z = 1$. Constant density for a uniformly charged $D = 3$ segment is represented by a thick red line.

We close this Section with a discussion of the direct calculation of the potential and the electric field as linear superpositions of the $d\Phi$'s and $d\vec{E}$'s due to infinitesimal bits of charge along the segment, $\lambda_D(z) dz$, for a line segment in D dimensions. In terms of the obvious rectilinear coordinates, as shown in Figure 14 of Section 4, the results are

$$\Phi_{\text{line}}(w, h) = k \int_{-L/2}^{L/2} \lambda_D(z) \left(\frac{1}{\sqrt{(h-z)^2 + w^2}} \right)^{D-2} dz, \quad (72)$$

$$\vec{E}_{\text{line}}(w, h) = (D-2) k \int_{-L/2}^{L/2} \lambda_D(z) \left(\frac{1}{\sqrt{(h-z)^2 + w^2}} \right)^{D-1} \hat{n} dz, \quad (73)$$

where w is the transverse distance from the segment and h is the z -coordinate of the observation point, and where $\hat{n} = \frac{\vec{r} - z\hat{z}}{|\vec{r} - z\hat{z}|}$ is a unit vector pointing from the location $z\hat{z}$ of the bit of charge on the segment to the observation point \vec{r} . Now, using the charge distribution (67) that produces ellipsoidal equipotentials, we eventually obtain

$$\Phi_{\text{line}}(w, h) = \frac{2k\lambda}{\Omega_D/\Omega_{D-1}} \left(\frac{2/L}{\sqrt{\sin\theta_b \sin\theta_t}} \right)^{D-3} \int_{\theta_b}^{\theta_t} \left(\sqrt{\sin(\vartheta - \theta_b) \sin(\theta_t - \vartheta)} \right)^{D-3} \frac{1}{\sin\vartheta} d\vartheta, \quad (74)$$

$$\vec{E}_{\text{line}}(w, h) = \frac{2k\lambda}{w} \frac{(D-2)}{\Omega_D/\Omega_{D-1}} \left(\frac{2/L}{\sqrt{\sin\theta_b \sin\theta_t}} \right)^{D-3} \int_{\theta_b}^{\theta_t} \left(\sqrt{\sin(\vartheta - \theta_b) \sin(\theta_t - \vartheta)} \right)^{D-3} \hat{n} d\vartheta, \quad (75)$$

where we have changed integration variables from z to an angle ϑ according to

$$z = h - w \cot \vartheta, \quad dz = \frac{w}{\sin^2 \vartheta} d\vartheta, \quad (76)$$

$$r = \sqrt{(h-z)^2 + w^2} = \sqrt{w^2 \cot^2 \vartheta + w^2} = \left| \frac{w}{\sin \vartheta} \right|, \quad (77)$$

$$\sqrt{\frac{1}{4} L^2 - z^2} = \frac{L}{2} \sqrt{1 - \frac{4}{L^2} (h - w \cot \vartheta)^2} = \sqrt{\frac{w^2 \sin(\vartheta - \theta_b) \sin(\theta_t - \vartheta)}{\sin^2 \vartheta \sin \theta_b \sin \theta_t}}. \quad (78)$$

Note that ϑ here is the polar angle *measured from the location of the bit of charge*, and in general this is not the θ shown in Figure 14 of Section 4. Nonetheless, θ_b and θ_t are the angles shown in Figure 14.

These last relations, in particular (78) and (75), are useful to establish *the direction of the electric field without actually performing the integration*. To verify this statement, let $\vartheta = \psi + \frac{1}{2}(\theta_b + \theta_t)$ in (75) to find

$$\vec{E}_{\text{line}}(w, z) = \frac{2k\lambda}{w} \frac{(D-2)}{\Omega_D/\Omega_{D-1}} \left(\frac{2/L}{\sqrt{\sin\theta_b \sin\theta_t}} \right)^{D-3} \int_{\frac{\theta_b - \theta_t}{2}}^{\frac{\theta_t - \theta_b}{2}} \left(\sqrt{\sin\left(\psi + \frac{\theta_t - \theta_b}{2}\right) \sin\left(\frac{\theta_t - \theta_b}{2} - \psi\right)} \right)^{D-3} \hat{n}(\psi) d\psi. \quad (79)$$

The integration here weights $\hat{n}(\psi)$ by an *even* function of ψ , with the range of integration symmetric about $\psi = 0$, so it follows that the resulting direction of $\vec{E}_{\text{line}}(w, h)$ will be proportional to $\hat{n}(\psi = 0) = \frac{1}{|\hat{r}_t + \hat{r}_b|} (\hat{r}_t + \hat{r}_b)$. That is to say, at any observation point around the segment the direction of \vec{E}_{line} bisects the angle formed by the two lines from the end points of the segment to the observation point, thereby confirming that the equipotentials are ellipsoids of revolution about the segment.

Note that this direct calculation of \vec{E}_{line} using the integral expression (79) generalizes prior calculations for $D = 3$ where the charge density is uniform, as given in [3, 4, 7, 8, 9], to cases where the charge distribution on the segment is *not* uniform for $D \neq 3$. We leave it as an exercise for the reader to evaluate the integral in (79) to obtain explicit expressions, and to show that these are in agreement with $\vec{E}_{\text{line}} = -\vec{\nabla}\Phi_{\text{line}}$. Even before attempting to evaluate the integral in (79), however, it should be evident that a determination of \vec{E}_{line} by taking the gradient of the potential is easier to carry through.

6 Generalizations

Having found the equipotentials for various charged line segments, we have in hand a set of solutions for a variety of electrostatic boundary value problems. If all the charge from the line segment is moved outward along electric field lines and placed on a single surface selected from among the equipotentials, in such a way as to preserve Φ on that surface, then the surrounding equipotentials are unchanged as well. This is widely known, and was in fact a feature emphasized by Green [1]. The charge distribution on the selected surface, as required to carry out this feat, is of course given by the electric field normal to that surface as provided by the original charged line segment solution. In particular, ellipsoidal equipotentials in any D yield hypersurface charge densities that are expressible as elementary functions. The results are straightforward generalizations of the well-known 3D ellipsoidal case.

In fact, it is not even necessary for the hyperellipsoids to be surfaces of revolution. For a general ellipsoid, as defined in D dimensions by

$$\sum_{n=1}^D \frac{x_n^2}{a_n^2} = 1, \quad (80)$$

the charge distribution on that hyperellipsoid such that it is an equipotential is given by

$$\sigma_D(\vec{r}) = \frac{Q}{\Omega_D \left(\prod_{n=1}^D a_n \right)} \frac{1}{\sqrt{\sum_{n=1}^D x_n^2/a_n^4}}. \quad (81)$$

This can be established by a straightforward adaptation of the argument that applies to the 3D case, as given for example in Smythe [5], Chapter 5, §5.00-§5.02.

If this charged hyperellipsoidal surface is “squashed” to obtain an equipotential hyperdisk (see Smythe §5.03 for the 3D case), say by letting $a_D \rightarrow 0$ while maintaining the constraint (80), then the hypersurface charge density on the resulting hyperdisk (counting charge on both sides of the disk) becomes

$$\sigma_D(r) = \frac{2Q}{\Omega_D \left(\prod_{n=1}^{D-1} a_n \right)} \frac{1}{\sqrt{1 - \sum_{n=1}^{D-1} x_n^2/a_n^2}}. \quad (82)$$

This charge distribution may now be projected along any of the remaining unsquashed principal axes of the original ellipsoid by elementary integrations. The final result is exactly the linear charge distribution given by (67), namely,

$$\lambda_D(x_k) = \frac{Q}{a_k} \frac{\Omega_{D-1}}{\Omega_D} \left(1 - \frac{x_k^2}{a_k^2} \right)^{\frac{D-3}{2}}, \quad (83)$$

where the projection has been made onto the k th axis. Alternatively, the surface charge distribution (81) of the unsquashed ellipsoid may be projected directly without being squashed, again by elementary integrations, to obtain the same result for λ_D .

7 Summary

In the context of a familiar subject — electrostatics — we have carried out several elementary calculations in various numbers of spatial dimensions, D , to encourage students to think more critically about the role played by D .

Although for $D = 3$ a uniformly charged straight-line segment gives rise to an electric potential Φ whose equipotential surfaces are prolate ellipsoids of revolution about the segment, with the ends of the segment providing the foci of the ellipsoid, this is a very special case. If $D \neq 3$, uniformly charged segments do not produce ellipsoidal equipotentials. If $D \neq 3$, a non-uniform distribution of charge is required to produce equipotentials that are ellipsoidal about a straight-line segment of charge.

We have illustrated these $D \neq 3$ features in detail for $D = 2$ and $D = 4$, and we have provided a framework as well as explicit formulas to carry through the same level of detail for any D . We have shown how $D = 2$ is the only ellipsoidal equipotential case which is intuitive in the sense that the associated linear charge distribution has maxima at the ends of the segment, as one might naively expect. In contrast, we have shown that the distribution of charge needed to produce ellipsoidal equipotentials is counter-intuitive for $D > 3$, becoming all the more so as D is increased, in the sense that the requisite charge distribution has an absolute maximum at the center of the segment and vanishes at its ends.

For $D = 3$ and $D = 4$, the potential surface plots were found to have similar features that can be distinguished only by careful inspection. Differences in Φ between uniformly charged line segments and those giving rise to ellipsoidal equipotentials were shown to be somewhat subtle. Distinctions between the two cases were more easily drawn by examining the corresponding electric fields close to the segment, or, relatedly, by directly comparing the charge densities.

We also took the opportunity to illustrate, albeit briefly, how continuous D can be viewed as a mathematical tool to regulate singular behavior and to interpolate between intuitive and counter-intuitive charge distributions. In the course of our discussion, we employed some basic geometrical ideas at an elementary level, such as in the determination of the direction of the electric field associated with ellipsoidal equipotentials.

Finally, we indicated how the line segment results may be generalized to solve a class of electrostatic boundary value problems by distributing the charge on hypersurfaces, rather than straight lines, while maintaining the line segment equipotentials outside the charged hypersurface.

Acknowledgement: We thank T S Van Kortryk for helpful discussions of the topics presented here.

References

- [1] G Green, *An Essay on the Application of Mathematical Analysis to the Theories of Electricity and Magnetism*, Nottingham (1828). Article 12. See pp 68-69 in [2].
- [2] N M Ferrers (editor), *Mathematical Papers of the Late George Green*, MacMillan and Company (1871). Especially p 329.
- [3] W Thomson and P G Tait, *Treatise on Natural Philosophy*, Part I & Part II, Cambridge University Press (1879 & 1883).
- [4] E Routh, *A Treatise on Analytical Statics with Numerous Examples*, Volume I & Volume II, Cambridge University Press, 1st edition (1891 & 1892).
- [5] W R Smythe, *Static and Dynamic Electricity*, McGraw-Hill, 2nd edition (1950).
- [6] A Sommerfeld, *Electrodynamics*, Academic Press (1952).
- [7] E Durand, *Electrostatique et Magnetostatique*, Masson et Cie (1953).
- [8] E Durand, *Electrostatique*, Volumes I, II, & III, Masson et Cie (1964).
- [9] P Gnädig, G Honyek, and K F Riley, *200 Puzzling Physics Problems: With Hints and Solutions*, Cambridge University Press (2001). See problem 117, p 28, and solution 117, pp 182-183.
- [10] A Zangwill, *Modern Electrodynamics*, Cambridge University Press (2013). See section 3.3.5, pp 65-67.
- [11] For more on the history of the 3D line segment problem, including citations of some recent pedagogical papers on the subject, see T S Van Kortryk, “On the fields due to line segments” arXiv:1410.6832 [physics.hist-ph].
- [12] Throughout our discussion we use rectangular Cartesian, spherical polar, and cylindrical coordinates, in view of student familiarity with these coordinate systems, even though prolate ellipsoids of revolution are more naturally described in terms of prolate spheroidal coordinates.
- [13] It is tempting to introduce the variable $t = r_+ - r_-$, the coordinate locally orthogonal to s in a prolate spheroidal coordinate system. This would make the result for \vec{E} just as compact as that for Φ_{line} when the equipotentials are ellipsoidal. However, the results are sufficiently manageable in terms of rectangular Cartesian coordinates, at least for graphical purposes, that there is no real numerical advantage achieved by using prolate spheroidal coordinates.
- [14] Beginning students can appreciate why the normal to a prolate ellipsoidal surface bisects the angle formed by the two vectors from the foci to any point on the ellipsoid by thinking about the law of reflection applied to a light ray that strikes an ellipsoidal mirror while en route from one focus to the other. Alternatively, a few banked shots on any good ellipsoidal billiard table should clarify the situation.
- [15] A Sommerfeld, *Partial Differential Equations in Physics*, Academic Press (1964).
- [16] Note that a careful limit of (37) is required to obtain the correct potential for $D = 2$. Just setting $D = 2$ in (37) would give a constant Φ .
- [17] The form in (61) is also more useful to obtain the correct result for $D = 2$ since the form in (57) requires taking a limit $D \rightarrow 2$ to obtain a nontrivial result.
- [18] Just how real conductors of finite length and girth reduce to uniformly charged ideal line segments in 3D is a venerable problem with a dignified history, beginning with J C Maxwell, “On the electrical capacity of a long narrow cylinder, and of a disk of sensible thickness” Proc. London Math. Soc. IX (1878) 94–101, reproduced as paper XCII, pp 672-680, in *The Scientific Papers of James Clerk Maxwell*, Vol. II, W D Niven, editor, Cambridge University Press (1890). For a guide to the literature since then, see J D Jackson, “Charge density on a thin straight wire: The first visit” Am. J. Phys. 70 (2002) 409-410. <http://dx.doi.org/10.1119/1.1432973>